Enhanced Vertical Orientation in Cylindrical PS-*b*-PMMA Using Ionic Liquid and Direct Immersion Annealing

by
Wafa Tonny

A thesis submitted to the program of Materials Science and Engineering,
Cullen College of Engineering
in partial fulfillment of the requirements for the degree of

MASTER OF SCIENCE
in Materials Science and Engineering

Chair of Committee: Dr. Alamgir Karim

Committee Member: Dr. Cunjiang Yu

Committee Member: Dr. Devin Shaffer

University of Houston
May 2020

ACKNOWLEDGMENTS

First and foremost, I would like to thank my research advisor, Dr. Alamgir Karim for his insight, leadership and inspiration to be a better researcher and student. Thank you for your continued support throughout this project as it could not have been completed without it.

Thank you Dr. Ali Masud for your time, effort and guidance during this project. His expertise on this field was the biggest help to complete the project. I am grateful and thankful.

I would like to express my gratitude towards Dr. Ali Ammar for his advice and important suggestions. I thank my colleagues and lab mates for their great help and guidance during this project. Thank you my friends especially Chuqing Yuan for his endless support and encouragement.

I would like to acknowledge that this thesis is a part of a project partially funded by National Science Foundation (NSF).

April 21, 2020

ABSTRACT

Block copolymer thin films have gathered much attention due to their well-defined structures and interesting surface morphology. Surface of the thin films depend on several factors like self-assembly of the polymers and interaction of polymer with solvent and substrate. The variables effecting the ordering of a block copolymer into perpendicular cylinder to the thin dimension of the film are crucial for its applications. This thesis presents a systematic study of ionic liquid (IL) as an additive on the perpendicular cylindrical ordering of a well-studied PS-*b*-PMMA (55K-22K) block copolymer (BCP) thin film. IL addition was varied in weight percentage of 0 – 15 relative to the mass of the BCP. Four different thickness of 40 nm, 100 nm, 200 nm and 400 nm of BCP films with varied concentration of IL were studied using atomic force microscopy (AFM) and grazing incidence small angle X-ray scattering (GISAXS) techniques. Contact angles were measured for 100 nm and 400 nm thick films to calculate surface energy. BCP films of four different thickness with IL additive were then annealed by direct immersion annealing (DIA) method. DIA was studied in a solvent mixture of toluene and heptane by varying volume ratio and immersion time. The variables were examined by using the same characterization techniques to explore the viability of the DIA method in attaining desired ordering of the BCP films.

TABLE OF CONTENTS

LIST OF TABLES

LIST OF FIGURES

CHAPTER I

Introduction

Self-assembling property of soft materials play an important role in meeting societal and economic goals for more efficient processes and smaller, hierarchically structured devices. Block copolymers are a class of self-assembling material that segregates on nanometer length scales, making them ideal for emerging nanotechnologies. Their application ranges from nanotemplating, nanoporous membranes, organic optoelectronics to anti-reflection coatings. These applications require the use of block copolymers in thin film geometries (~100 nm thickness), where self-assembly is strongly influenced by surface energy. Decades of research have provided a foundation for understanding block copolymer self-assembly, beginning with the characterization of bulk morphologies using the Flory-Huggins interaction parameter (χ), degree of polymerization (N), block volume fractions (f) and chain architecture (e.g., linear, star, etc.). Recent literature has provided a working knowledge of surface energy effects in block copolymer thin films (e.g., on microstructure orientation and phase transformations); however, a better understanding of thin film nanostructures is still a significant research focus.[1] Control of the subsequent annealing conditions to obtain the desired ordered block copolymer (BCP) morphology is key to achieving a target degree of ordering. Several annealing techniques are prevalent now such as thermal annealing and solvent vapor annealing. Thermal annealing involves simply heating the BCP films above the glass transition temperature (T_g) of both blocks to provide sufficient mobility to allow BCP ordering on a reasonable time scale. Thermal annealing can be disadvantageous if one or more blocks can crystallize or if the blocks chemically degrade

at the elevated annealing temperatures. The slow diffusion of high molecular mass polymers also increases the BCP film processing time. Solvent vapor annealing (SVA) of BCP films overcomes some of the drawbacks of thermal annealing, but introduces new challenges. The thin films swell when exposed to vapor where the extent of swelling depends on the nature and amount of solvent adsorbed. The film swelling can lead to a number of undesirable effects that are difficult to control. The extent of film swelling resulting from the processing conditions can affect morphology, domain size and the orientation of BCP morphology with respect to substrate. Other effects can include dewetting, differential block swelling and shifts of order−disorder or order−order transitions that depend sensitively upon the solvent and processing conditions.[2] Direct immersion annealing (DIA) is a fairly new directed self-assembly technique. Unlike solvent vapor annealing, DIA orders BCP films as they are directly submerged in bulk solvent. This eliminates any need for generating vapors or carefully controlling vapor pressures as it is required in SVA. DIA requires a specific solvent quality for the BCP film that is tunable via a miscible solvent mixture. A large fraction of poor solvent for the BCP film prevents film dissolution, while a low fraction of good solvent enables limited film swelling and molecular mobility for ordering. The presence of solvent during the ordering process introduces a tunable feature with potential for improving BCP structure, feature size, and kinetics.[3] In addition to different annealing techniques plasticizers have interesting attributes in polymer blend. An exceptional effect of ionic liquids (ILs) as plasticizers have been garnering attention. ILs show compatibility with synthetic polymers contributing to the self-assembly which helps in manufacturing functional soft materials without any drastic effect on the properties.[4]

This work reports the effect of addition of a particular IL on the self-assembly of a known and useful block copolymer poly (styrene-*b*-methyl methacrylate) (PS-*b*-PMMA) and further investigating the impact of DIA on the same system. Vertical orientation of a block in the polymer matrix perpendicular to the substrate is highly advantageous for future advanced application. The choice of IL and the role of IL in specific orientation of PS-*b*-PMMA has been studied. The results of DIA techniques with proper analysis on the polymer and IL blend matrix has been reported here. Economical and safe techniques play an essential part in improvements of the directed self-assembly research and that is the motivation of this thesis.

CHAPTER II

Literature Review

The thermodynamic driving force that leads to segregation of the two chemically disparate polymer blocks lies at the center of self-assembly system. At equilibrium, the ordered state symmetry and sizes of the structures that emerge from the self-assembly process are largely governed by the volume fraction of each block i.e., composition, f_i and the overall degree of polymerization, N of the block polymer which is proportional to the molar mass. However, enough incompatibility between the constituent monomers is required for self-assembly. Following the most modern interpretations of Flory−Huggins theory, it is convenient to combine all excess thermodynamic contributions to the overall free energy i.e., enthalpic and noncombinatorial entropic factors into an effective interaction parameter denoted χ_{eff}. Mean-field theory predicts that symmetric AB diblock copolymers ($f_A = 1 - f_B = 1/2$) will produce ordered structures when the product $\chi_{eff}N$ (using a value of N based on a common segment reference volume, $v_A = v_B$) is greater than 10.5. Thus, at fixed χ_{eff}, there is a minimum value of N necessary for self-assembly. The degree of phase separation in the BCP is dictated by the product of χ and N. In general, the larger the value of χN, the higher is the degree of phase separation.[5] If they are amphiphilic, BCPs in melts spontaneously separate into two phases to minimize the Gibbs free energy of mixing. This phenomenon is mainly explained by the Flory−Huggins model, based on the interaction energies between A and B monomers and the entropy of the arrangement of polymer chains,

$$\Delta \boldsymbol{G_{mix}} = \Delta \boldsymbol{H_{mix}} - \boldsymbol{T}\Delta \boldsymbol{S_{mix}}$$

$$= kT\,[\chi f_A\,(1- f_A) + \frac{f_A}{N_A}\ln f_A + \frac{1-f_A}{N_B}\ln(1- f_A)],$$

where ΔG_{mix}, ΔH_{mix}, and ΔS_{mix} are the Gibbs free energy, enthalpy, and entropy of mixing, respectively, T is the absolute temperature, k is the Boltzmann constant, f_A is the volume fraction of the A monomer, N_A and N_B are the polymerization degrees of the A and B monomers, respectively, and χ is the enthalpic interaction parameter between the A and B monomers (χ parameter; higher χ promotes phase separation).[6]

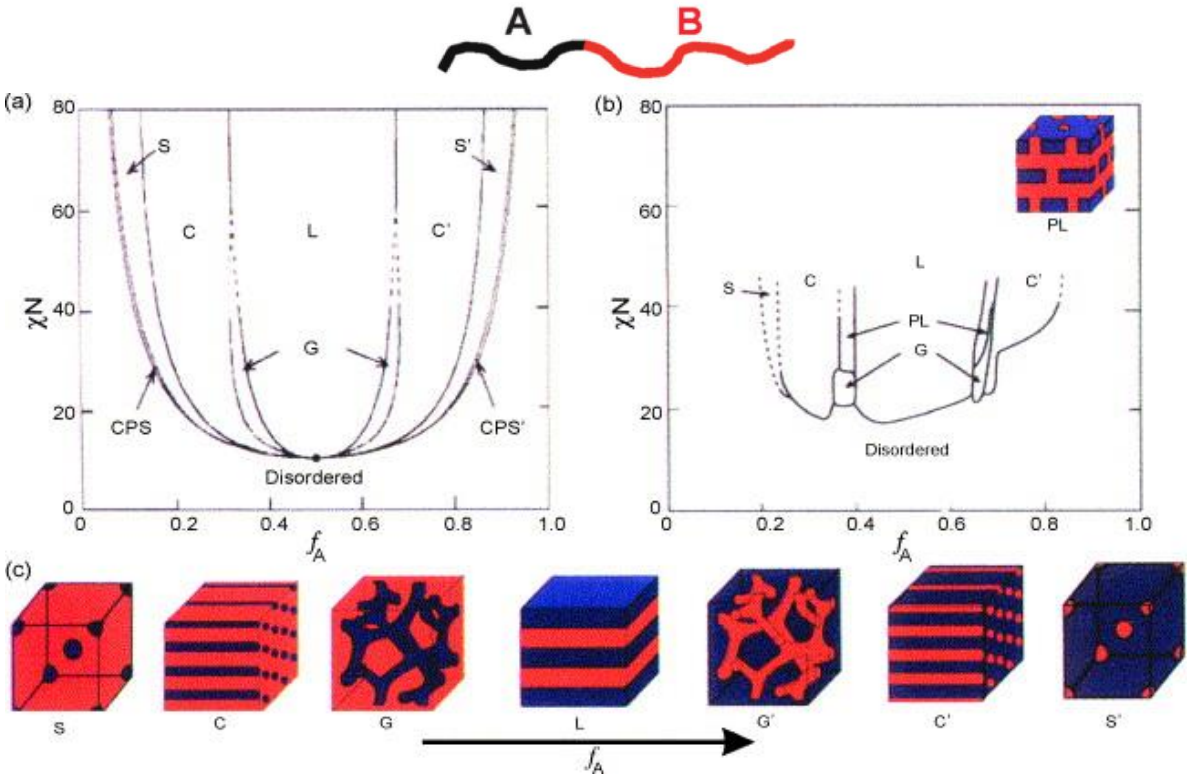

Figure 1: Diblock copolymers are predicted to self-assemble according to a phase diagram predicted by self-consistent meanfield theory (a) and proven experimentally (b). (c) A variety of constant-radius geometries are observed as a function of relative lengths of the two blocks (c) spherical (S), cylindrical (C), gyroid (G) and lamellar (L) structures.[6]

A symmetric diblock copolymer is predicted to disorder (or pass through its order–disorder temperature (ODT)) when $\chi N < 10.5$. Below the ODT and when the volume fraction of block A (f_A) is quite small, it forms spheres in a body-centered cubic

(BCC) lattice surrounded by a matrix of B. As f_A is increased towards 0.5, the minority nanodomains will form first cylinders in a hexagonal lattice, then a bicontinuous double gyroid structure, and finally lamellae. The size and periodicity of the nanodomains are also functions of the polymer size (N) and the segmental interactions (χ), as shown in Figure 1.[6]

In general, $\chi = \frac{a}{T} + b$,

where a and b are experimentally obtained constants for a given composition of a particular blend pair. Experimentally, χ can be controlled through temperature. Unlike macrophase separation in blends, the connectivity of the blocks in block copolymers prevents complete separation and instead the diblock copolymer chains organize to put the A and B portions on opposite sides of an interface. The equilibrium nanodomain structure must minimize unfavorable A–B contact without over-stretching the blocks.

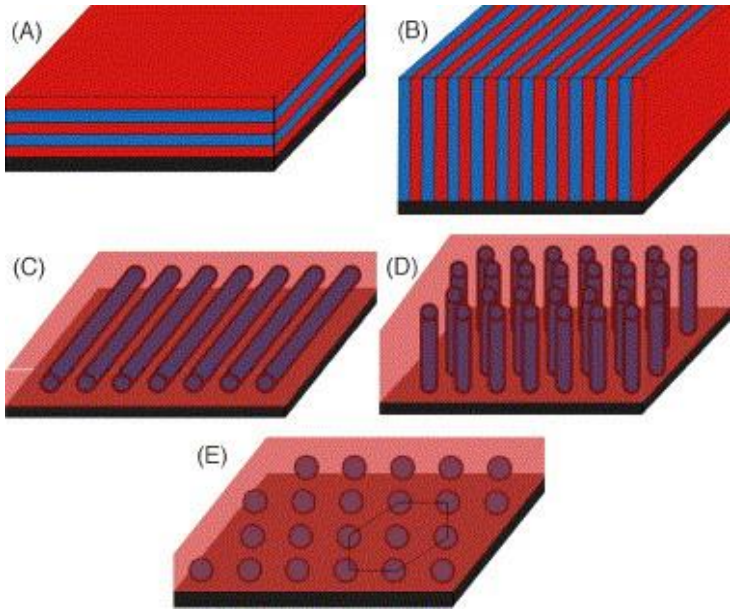

Figure 2: (A) Lamellae lying parallel to the substrate (B) lamellae aligned perpendicular (C) cylinders lying parallel (D) cylinders perpendicular and (E) spheres.[6]

When confined to a thin film, the orientation of block copolymer domains with respect to the substrate surface is crucial for many applications. In the case of lamellae in the perpendicular orientation and cylinders in parallel, lines can be patterned if the persistence length of the structure can be controlled. In the case of upright cylinders and spheres, the grain size and perfection of the hexagonal array is of primary importance.[6]

Role of Ionic Liquid (IL)

A conceptually different role of an ionic liquid (IL) additive is that it increases the χ_{eff} of BCP such as poly (styrene-*b*- methyl methacrylate) (PS-*b*-PMMA) without radically changing the advantageous surface and interfacial properties of PS-*b*-PMMA. A selective IL additive only goes into the polar PMMA domains, thus boosting the χ_{eff} between the blocks. One paper promoted that the phase separation of PS-*b*-PMMA in thin films by the addition of 1-ethyl-3-methylimidalzolium bis(trifluoro-methanesulfonyl) amide ([EMIM][TFSI]) (molecular weight of 391.30). This enhanced phase segregation of BCPs upon the addition of ILs may provide a promising approach to enable the directed self-assembly of PS-*b*-PMMA below its intrinsic resolution limit of 10 nm.[7]

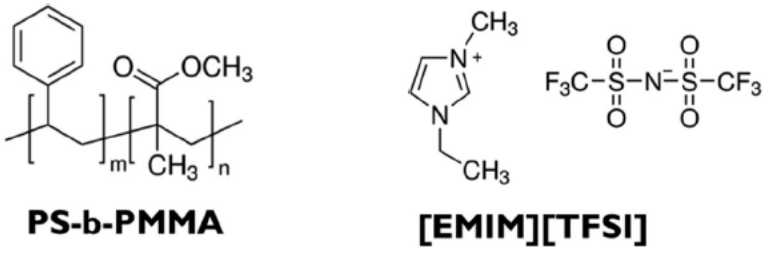

Figure 3: Structure of the PS-b-PMMA block copolymer and the IL 1-ethyl-3-methylimidazolium bis (trifluoromethyl sulfonyl) imide ([EMIM][TFSI]).[7]

The IL additive is selectively soluble with the more polar PMMA domain when being blended with PS-*b*-PMMA, thus increasing the polarity of its resident block and enhancing the segregation strength between the two blocks. Owing to the low concentration, the IL additive does not significantly change the surface in the thin film. Several additional criteria in the selection of ILs to blend with BCPs for direct self-assembly in that published work included a propensity to increase χ_{eff}, ability to control domain orientation and good thermal stability.[7]

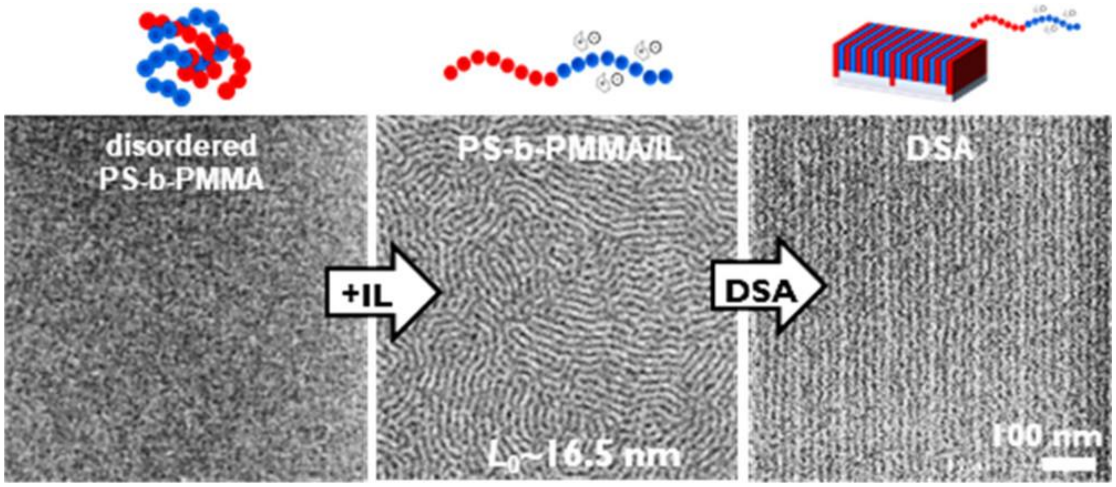

Figure 4: IL incorporated direct self-assembled (DSA) PS-*b*-PMMA thin film with vertical lamellar structure.[7]

The combination of anions and cations with weak Lewis acidity and basicity forms salts with low melting temperatures, i.e., room-temperature ionic liquids (ILs). ILs, composed entirely of ions, exhibit unique properties such as thermal and electrochemical stability, negligible volatility, non-flammability, and high ionic conductivity. ILs are generally regarded as novel green solvents, applicable to the extraction, partition, and separation of various target molecules and as electrolytes for electrochemical devices. The properties of ILs can be designed by the combination of cations and anions, which

enables tuning of the properties, including hydrophilicity and hydrophobicity, Lewis acidity and basicity, and hydrogen bonding ability. ILs also exhibit good compatibility with various synthetic polymers, allowing the preparation of functional soft materials.[4] An anomalous plasticizing effect was observed in polymer/ionic liquid (IL) solutions by applying broad range of rheological techniques. As an example a poly (ethylene oxide) (PEO)/IL solutions exhibit stronger dynamic temperature dependence than pure PEO, which is in conflict with the knowledge that lower-T_g solvent increases the fractional free volume. For poly (methyl methacrylate) (PMMA)/IL solutions, the subtle anomaly was detected from the fact that the effective glass transition temperature $T_{g,eff}$ of PMMA/IL is higher than the prediction of the self-concentration model, while in conventional polymer solutions, $T_{g,eff}$ follows the original Fox equation. Observations in both solutions reveal retarded segmental dynamics, consistent with a recent simulation result [8] that polymer chains wrap the IL cations by hydrogen bonding interactions and the segmental unwrapping delays their relaxation. Start-up shear and nonlinear stress relaxation tests of polymer/IL solutions follow a universal nonlinear rheological behavior as polymer melts and solutions, indicating that the segment-cation interaction is not strong enough to influence the nonlinear chain orientation and stretch.[9]

Direct immersion annealing (DIA)

A poor solvent is chosen as one of the solvents to regulate the rate of polymer film dissolution, along with a good solvent that imparts high degree of mobility within the film. The overall mixture then maintains a finite interaction parameter for micro phase separation.[2]

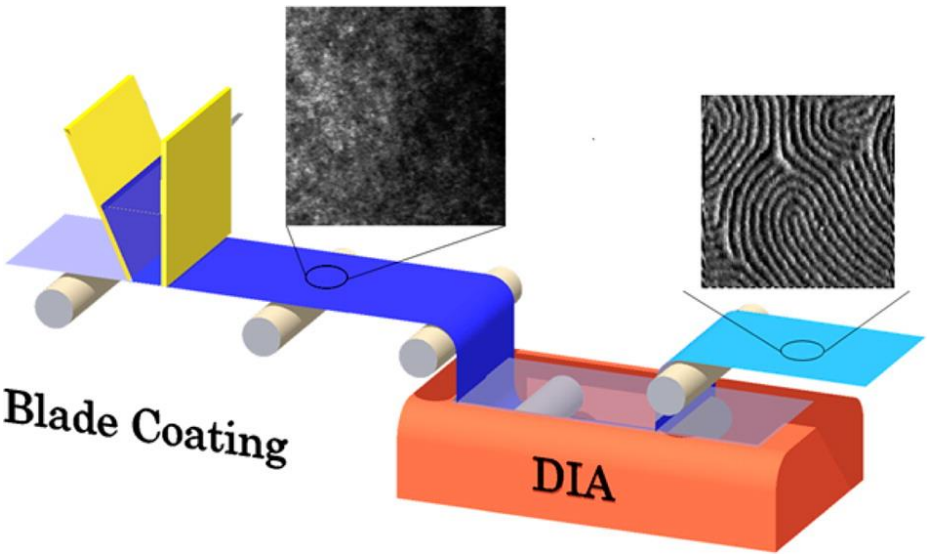

Figure 5: Direct Immersion Annealing (DIA).[2]

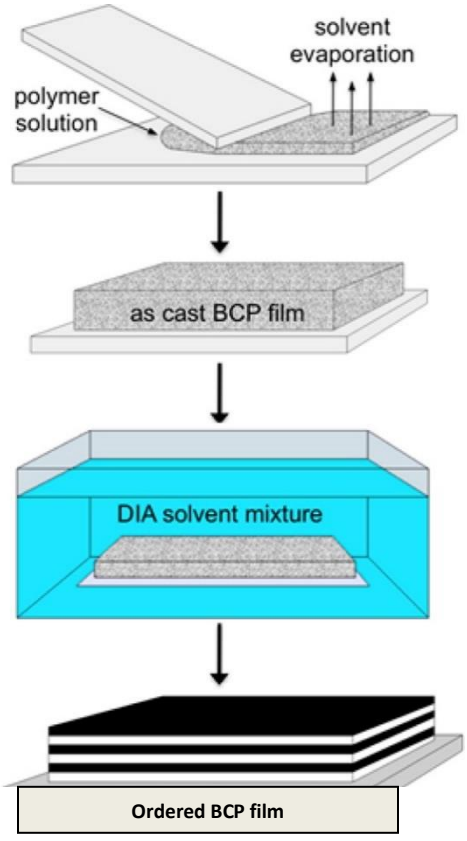

Figure 6: Schematic of direct immersion annealing (DIA) process.[2]

A great demonstration of DIA was on a published paper with poly(styrene-*b*-dimethylsiloxane) (PS-*b*-PDMS) as a model system for high-χ BCPs with a known χ parameter of 0.26 at room temperature which is at least several times larger than that of PS-*b*-PMMA.[10]

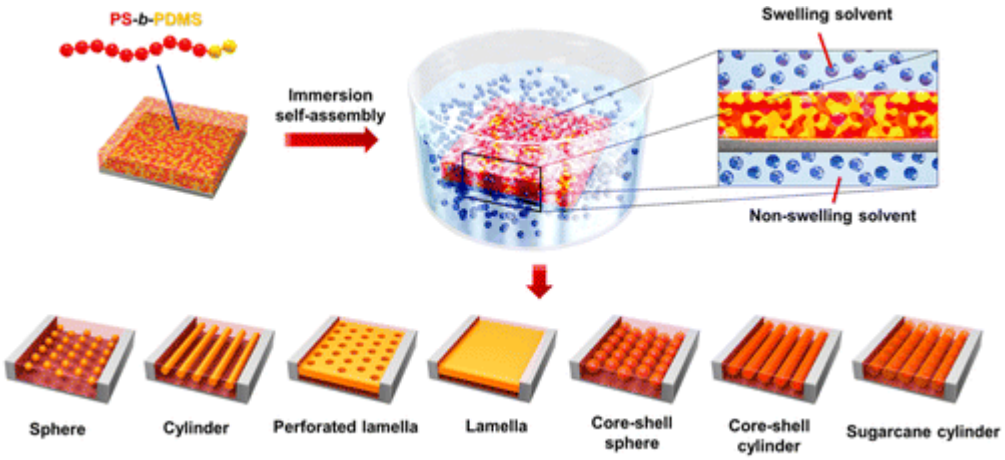

Figure 7: Schematic of immersion-triggered self-assembly.[10]

A BCP film is immersed into the mixture of swelling and nonswelling solvents. The swelling solvent molecules penetrate into the BCP film and induce the self-assembly process. Various self-assembly nanostructures, such as spheres, cylinders, perforated lamella, lamellae, core-shell spheres, core-shell cylinders and sugar cane cylinders can be formed from one BCP i.e., PS-*b*-PDMS.[10]

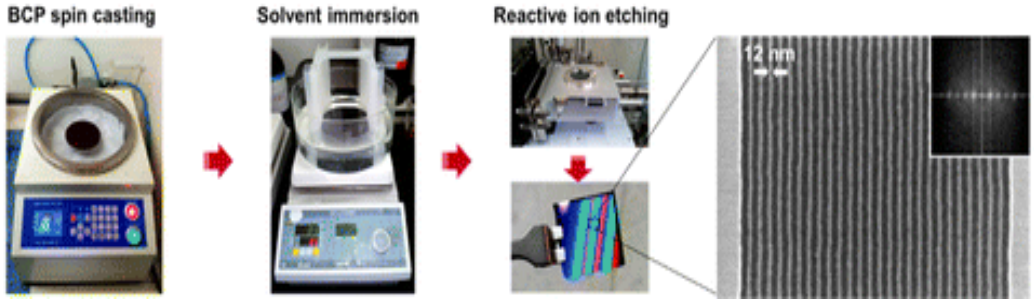

Figure 8: Procedure of the direct self-assembly method for PS-b-PDMS system.[10]

This method presented here consisted of BCP spin-casting, immersion in the solvent mixture, and reactive ion etching to remove the PS and to oxidize the PDMS. The scanning electron microscopy (SEM) image shows line and space patterns prepared from the BCP.[10]

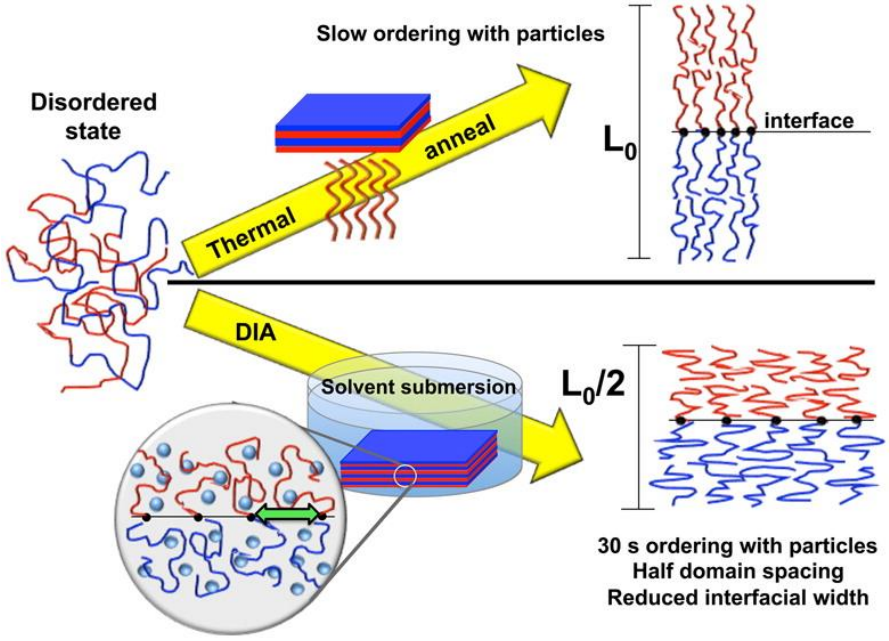

Figure 9: An illustration for a system of 33− 33 kg/mol PS-*b*-PMMA filled with 10.5 vol % AuNP (Nano Particles) used the advantageous features of DIA method.[3]

The system described in **Figure 9** explained that the presence of solvent during self-assembly gives rise to unique BCP behavior such as reduced and in general, tunable interfacial widths as well as highly reduced domain spacing that has thus far not been observed for conventional annealing techniques. The ability to control interfacial widths by tuning and selecting solvents that can alter the interaction parameter between two blocks of a BCP serves as a mechanism to produce self-assembled structures with sharp interfaces. Specifically, a reduction in interfacial width of 15% in both loaded and nonloaded films was observed for the ternary solvent mixture and 22% for the two-solvent system of higher selectivity. This is a promising result for applications of neat

BCP films in nanoelectronics as well as a cleaner templating route for organization of particles.[3]

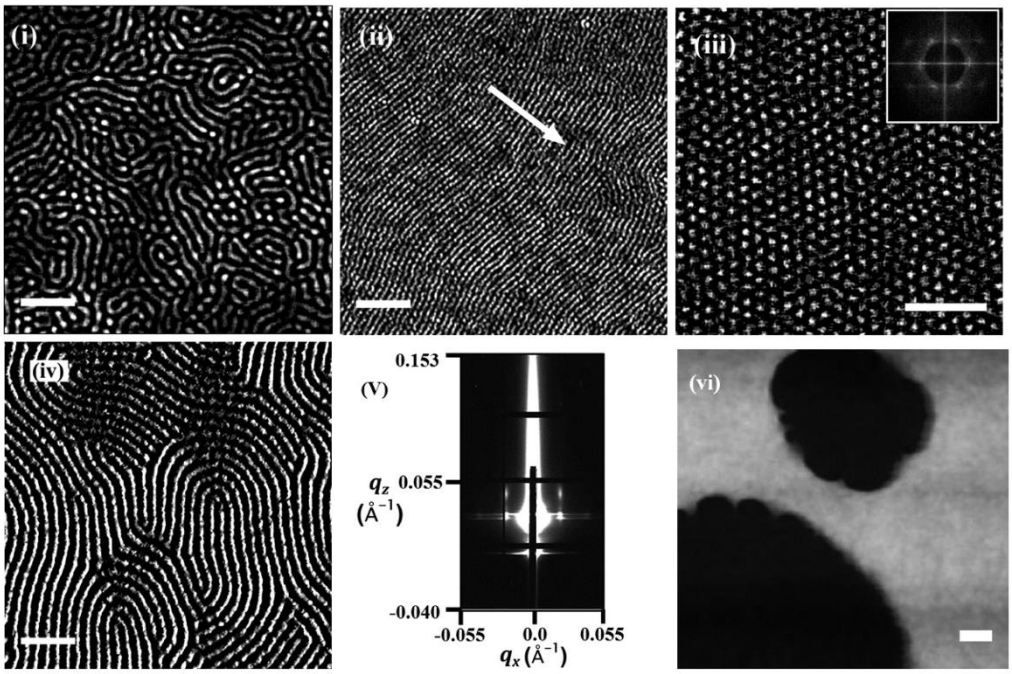

Figure 10: Atomic force microscopy (AFM) images to illustrate applicability of DIA to other block copolymer systems and PS-*b*-PMMA with different molecular parameters.[2]

In **Figure 10** the AFM images illustrate the applicability of DIA to other block copolymer systems and PS-*b*-PMMA with different molecular parameters. **Figure 10 (i)** shows randomly oriented, but ordered poly (styrene-*b*-2vinylpyridine) (PS-*b*-P2VP), (40−18 kg/mol) annealed for 1 h in a solvent mixture of acetone and heptane composed of x_{ace} = 0.40. Atomic force microscopy (AFM) shows in-plane long-range ordered cylinders [**Figure 10 (ii**)] that on average are aligned orthogonal to the PDMS channel pattern shown by the arrow in a direction parallel to the pattern ridges. **Figure 10(iii)** shows AFM height image of a spherical PS-*b*-PMMA (60−15 kg/mol) film immersed in a ternary solvent mixture composed x_{ace} = 0.57, $x_{heptane}$ = 0.38 and $x_{toluene}$ = 0.05 for 1 h and dried on hot-plate at 60 °C. The inset 2D FFT of the AFM image is indicative of a highly

ordered hexagonal packing structure. **Figure 10(iv)** shows AFM height image of a cylindrical PS-*b*-PMMA (57−25 kg/mol) film immersed in a solvent mixture composed of x_{ace} = 0.57 for 1 h and dried on a hot-plate at 60 °C. **Figure 10(v)** shows sharp Grazing incidence small angle X-ray scattering (GISAXS) spot pattern in q_x and q_z indicative of high degree of in-plane and out-of-plane cylinder-cylinder correlation for a PS-*b*-PMMA (47.5 kg/mol) film annealed in solvent mixture of x_{ace} = 0.21, $x_{methyl\ ethyl\ ketone}$ = 0.17 for 1 minute. **Figure 10(vi)** shows AFM height images of lamellar PS-*b*-PMMA (33−33 kg/mol) film annealed in a mixture composed of x_{ace} = 0.57 and $x_{toluene}$ = 0.05 for 45 minutes.[2]

CHAPTER III

Experimental Methods

Materials

Block Copolymer (BCP): Poly (styrene-*b*-methyl methacrylate) (PS-*b*-PMMA); molecular weight of 77,000 (PS block - 55,000 and PMMA block – 22,000) as received from Polymer Source. Inc.

Ionic liquid (IL): 1-ethyl-3-methylimidazolium bis (trifluoromethyl sulfonyl) imide ([EMIM][TFSI]); molecular weight of 391.30 as received from Tokyo Chemical Industry Co. Ltd.

Solvents: Toluene (anhydrous, 99.8%), Heptane (anhydrous, 99%), Methanol (anhydrous, 99.8%) and Tetrahydrofuran (anhydrous, ≥ 99.9%, inhibitor-free) (for IL) as received from Sigma-Aldrich.

Film Casting Method

PS-*b*-PMMA films were flow coated on the Silicon substrate wafers with the native SiO_2 layer. There are few techniques to coat or cast a polymer film. Flow coater is one of the efficient ones because films of various thickness can be coated fast. Usually a flow coater has a fixed blade and a moving stage. The residue polymer solution at the edge of the blade is taken up by the capillary force. So it is directly dependent of the gap between the stage and the blade, which is about 10 μm. Then the speed of the moving stage determines the thickness of the films coated. The concept here is that if the speed is higher, the thickness of the coated film will also increase. A clean glass slide was used as

the blade. Substrate was silicon wafer. A motion control software from 'GalilTools' was used to control the speed of the stage.

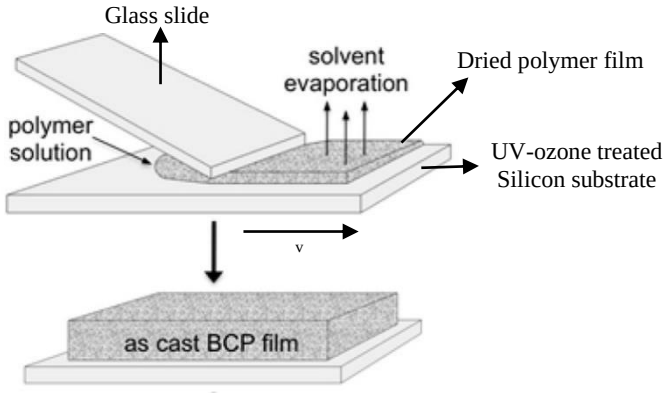

Figure 11: A schematic of flow coating technique.[2]

The silicon wafer was cut into desired length by a diamond cutter and was cleaned by blowing air on to the piece. To reduce the contamination silicon wafer was treated in ultraviolet-ozone (UV-ozone) chamber. The UV-ozone cleaning procedure is an effective method to remove a variety of contaminants from substrate surfaces. UV Radiation will hit the polymer surface and excite the polymer surface or organic contaminant to generate radicals to enable them react with ozone. It is an efficient way to remove organic contaminations and also to increase the surface energy of the substrate which is helpful to coat a film where UV line decomposes ozone and produces high energy O* (activated oxygen).

Film Thickness Measurement by Interferometer

Interferometers are widely used for the measurement of small displacements, refractive index changes and surface irregularities. In most interferometers, light from a single source is split into two beams that travel in different optical paths, which are then combined again to produce interference. The resulting interference fringes give

information about the difference in optical path lengths. The interference between light waves is the reason thin films show colorful pattern. The light waves reflecting off the top surface of the film and the light waves reflecting off from the bottom of the film or more accurately from the surface of the silicon wafer create interference. The thickness of the film has to be similar to the wavelength of the light to show a color pattern. Taking an account of the refractive index value of PS-*b*-PMMA film and the interference of the reflective lights, the interferometer determines the thickness of the film. The interferometer used to measure the thickness was F-3 UV made by Filmetrics and the model was LS-DT2.

Atomic Force Microscopy (AFM)

Atomic force microscopy (AFM) is widely used for measuring surface morphology, mechanical, electrical and magnetic properties of nanostructured materials and monitoring chemical changes over surfaces due to the benefits of nanometer spatial resolution and high sensitivity. It is type of scanning probe microscope which permits three dimensional characterizations with sub-nanometer resolution. It uses a sharp tip scanned over the specimen to sense surface forces. In principle, either attractive or repulsive forces between the tip and surface can be detected; in practice, the repulsive force mode is predominantly used because it is more stable. The microscopic image produced is that of a surface, representing the locus of points of constant force between the tip and the specimen.[11] What is measured is deflection of the tip, which can be recorded and convert to a height. The deflections caused by this force allow the AFM to record topographic features of the surface. The device measures vertical as well as lateral sizes of nanostructures. The vertical dimension of the feature approach the real height;

however, the lateral dimensions are actually convolution of the dimension of the feature with the diameter of the tip.[12]

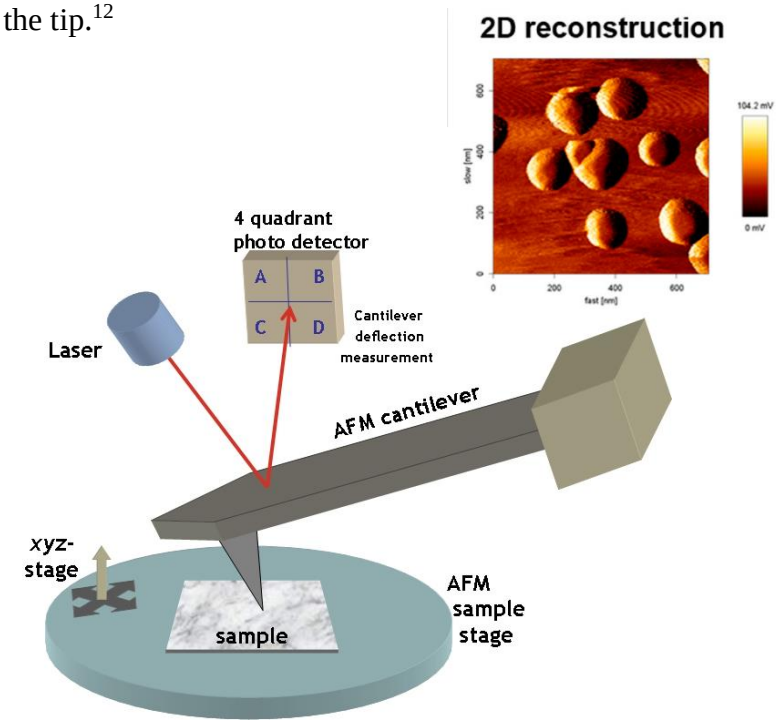

Figure 12: An AFM setup.[13]

The AFM typically operate in one of two modes- contacting mode with the tip contacting the specimen and noncontacting or tapping mode. In tapping mode, the cantilever is externally oscillated close to its resonance frequency. The vibration characteristics of the cantilever beam is influenced by the tip-sample interaction forces; these changes in oscillation provide information about the specimen geometry.[14] AFM enables any measurements that requires the sample height such as thickness or roughness to be measured accurately and with very high resolution. The AFM can provide a true three-dimensional map of the surface. For the work of this thesis, Bruker Dimension Icon AFM with ScanAnalyst in standard tapping mode over scan size 2µm × 2µm at scan rate of 0.99 Hz in air has been used to scan the films.

Grazing Incidence Small Angle X-Ray Scattering (GISAXS)

To confirm the chain orientations of casted thin film, grazing incidence small angle X-ray scattering (GISAXS) experiments were carried out in Beamline 8-ID-E of advanced photon source in Argonne National Lab. GISAXS patterns at different incidence angles give detailed information for the morphology of thin BCP film on a silicon substrate. Since the X-ray beam impinges only near the surface region which is the below the critical angle of the film (0.12°), the details on the depth dependence of the thin-film morphology are easily investigated by controlling the incident angle. For most studies, a series of incident angles ranging from 0.14° to 0.16° are used to achieve penetration depths from the top surface less than 10 nm to the full penetration in the films.[15]

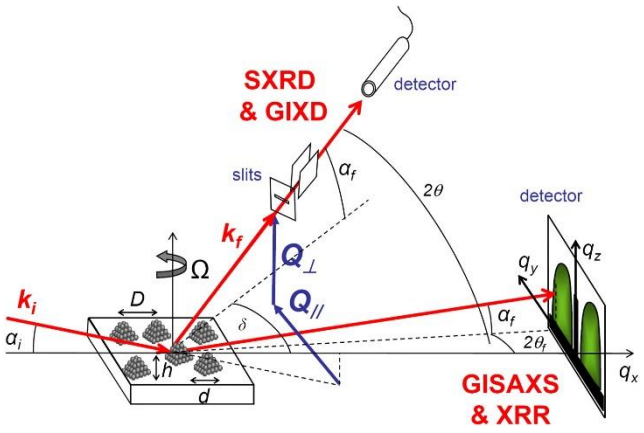

Figure 13: GISAXS geometry.[16]

GISAXS provides information both about lateral and normal ordering at a surface or inside a thin film. In a block copolymer two immiscible polymer chains are coupled by a chemical bond. If both chains occupy equal volumes, a lamellar phase is formed.

In a thin film, i.e., if the thickness of the film is on the order of the lamellar period, the presence of two interfaces, air-film and film substrate, may induce preferential order in the film as compared to the bulk polymer which forms a 3D powder of micron-sized lamellar domains. If interfacial energies are the dominant factor, i.e., if one of the block strongly favors the interface, parallel lamellae are formed. If the interfacial energies of the blocks are similar, interfacial entropy will determine the orientation of the blocks.

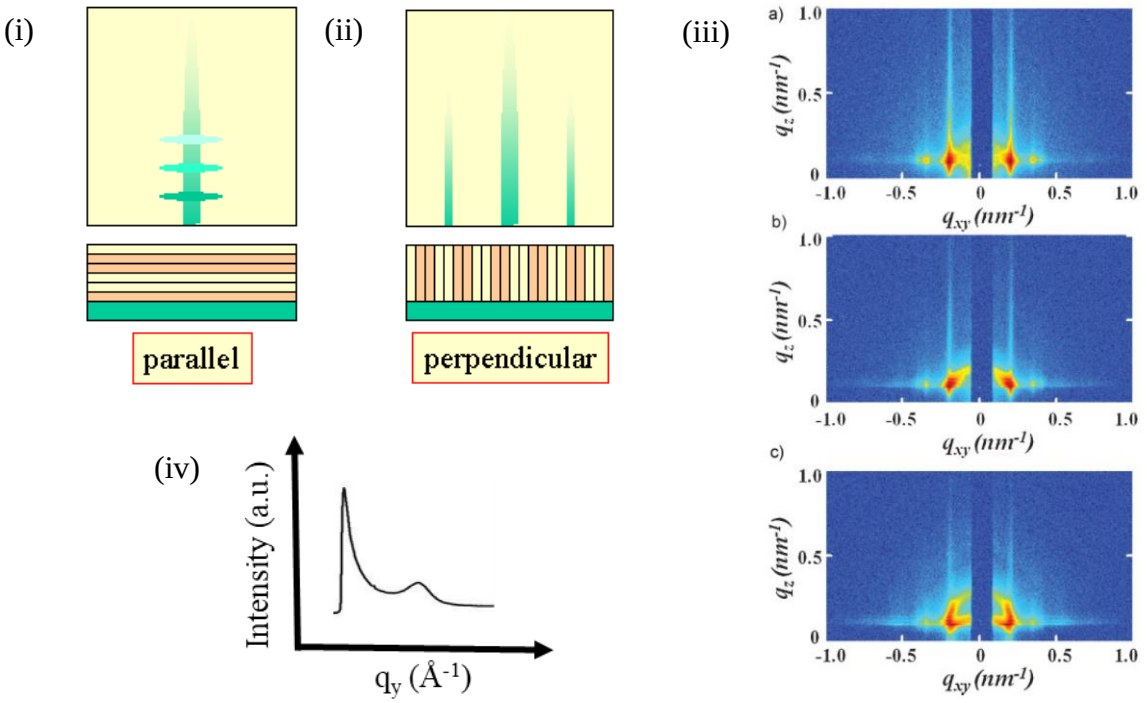

Figure 14: The signature in GISAXS pattern (i) for parallel lamellae-stripes of intensity at regular spacings along the q_z direction[17] (ii) for perpendicular lamellae- rod-like shape normal to the surface[18] (iii) 2D GISAXS patterns at various incidence angles for a nano-porous PS-*b*-PMMA film on silicon substrate. The incidence angles are a) 0.11°, b) 0.12°, and c) 0.15°[15] (iv) a standard in-plane linecut profile (intensity vs. q, the scattering vector in y direction).

If one of the blocks strongly favors one of the two interfaces, or even both, the lamellae will be parallel to the substrate. The classic example is PS-*b*-PMMA on a Si wafer covered with the native oxide layer. The signature of parallel lamellae in GISAXS are stripes of intensity at regular spacing along the q_z direction.[17] The signature of

perpendicular lamellae is correlation peaks parallel to the interface, with a rod-like shape normal to the surface.[18]

Surface Energy and Contact Angle

Measuring the surface energy is an important task to determine surface wettability and selecting polymer-solvent-substrate combination. Over time many scientists have attempted on calculating surface energy. Some of the famous theories are Zisman theory, Van Oss theory and Fowkes theory. For this work Fowkes theory was used. According to this concept, Surface energy of a polymer film has two components: a dispersive component and a polar component[19]. The primary equation of the Fowkes surface energy theorem is:

$$2(\sigma_L^D)^{1/2}(\sigma_S^D)^{1/2} + (\sigma_L^P)^{1/2}(\sigma_S^P)^{1/2} = \sigma_L(cos\,\theta + 1).$$

Here, $\sigma_L{}^D$ is the dispersive component of the surface tension of the wetting liquid, $\sigma_L{}^P$ is the polar component of the surface tension of the wetting fluid, $\sigma_S{}^D$ is the dispersive component of the surface energy of the solid and $\sigma_S{}^P$ is the polar component of the surface energy of the solid. Fowkes theory is applicable using contact angle data from two liquids. Diiodomethane and deionized water were used in the contact angle measurement. Fowkes theory is based on three fundamental equations which describe interactions between solid surfaces and liquids. One of them is Young's Equation:

$$\sigma_S=\sigma_{SL}+\sigma_L\cos\theta,$$

where, σ_L = overall surface tension of the wetting liquid

σ_S=overall surface energy of the solid

σ_{SL}=the interfacial tension between the solid and the liquid

θ=the contact angle between the liquid and the solid

Ablation test by UV (Ultra-Violet) etching

This test named this way because by non-selective etching of the thin films the thickness is reduced. To determine in detail, the orientation of cylindrical nanopores throughout the entire film, UV-ozone technique was performed which can etch the film from the surface with an accuracy of nanometer scale. In literature before the etching, for PS-*b*-PMMA film vertically oriented cylindrical nanopores were observed in both top and bottom sides of the film but the inner part of the film shows mixed orientation of cylindrical nanopores. The etched rate was determined to be $2nms^{-1}$.[15]

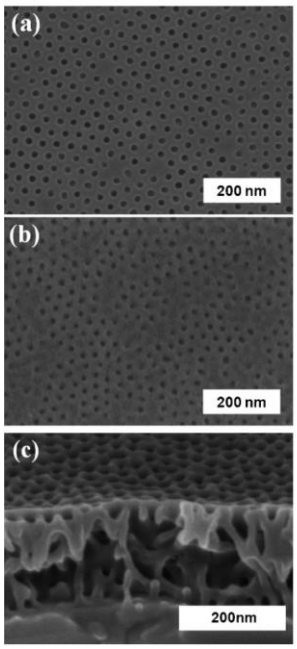

Figure 15: SEM images for a nanoporous film prepared by PS-*b*-PMMA after UV-ozone etching followed by rinsing with acetic acid a) Top surface b) bottom surface and c) cross-sectional view.[15]

CHAPTER IV

Results and Discussions

As Cast Film

2wt% IL solution was added in the 2% PS-*b*-PMMA (55K-22K) solution in varying percentage of 0-15%. The BCP-IL mix solution was then flow coated to give films of 100 nm thickness. The fabricated as-cast films were in a quenched-disordered state.[20] The thickness was measured, and the films were properly dried under vacuum overnight at 60°C (well below glass transition temperature or degradation temperature). Then the surface of the films was scanned by AFM to analyze the orientation of the PMMA phase. GISAXS data were also collected to analyze the orientation in film thickness.

As Cast PS-*b*-PMMA film with IL*: Effect of IL (wt%) concentration*

Film thickness: 100 nm

IL (wt%): 0%, 2%, 4%, 5%, 8%, 12%, 15% in 2% PS-*b*-PMMA(55K-22K)

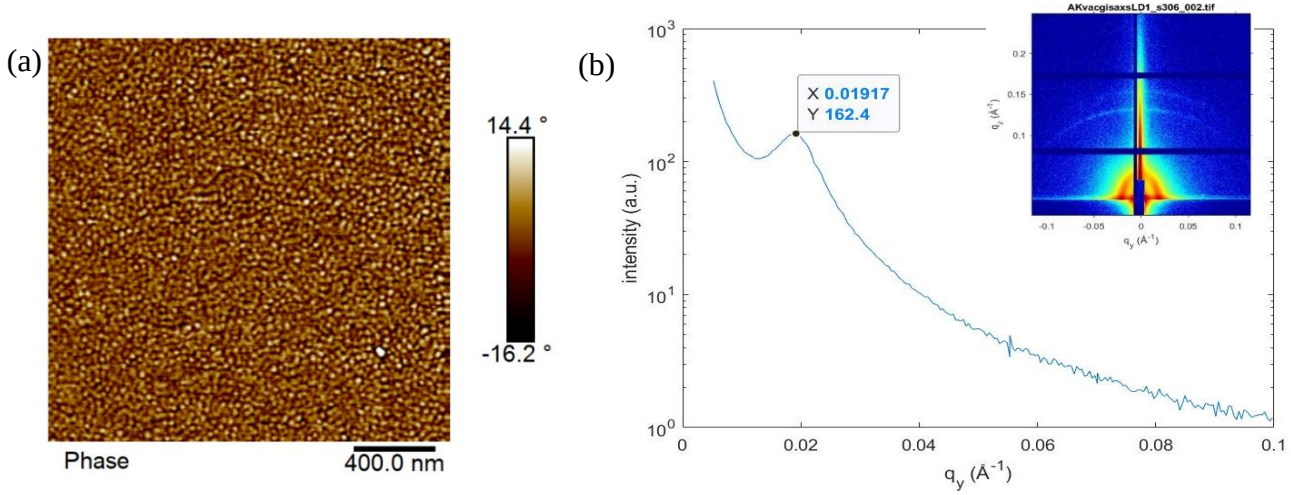

Figure 16: (a) AFM scan image and (b) In-plane scattering profiles of horizontal cut of inset 2D GISAXS pattern of 0wt% IL in 2% PS-*b*-PMMA(55K-22K).

As cast 100 nm 2% PS-*b*-PMMA(55K-22K) film without any IL showed no orientation. The AFM phase image and the GISAXS pattern explained that. The calculated domain spacing from the in-plane scattering profile using the equation of domain spacing, d= $2\pi/q^*$, where q^* is the maxima taken at the first order peak was 32.7 nm.

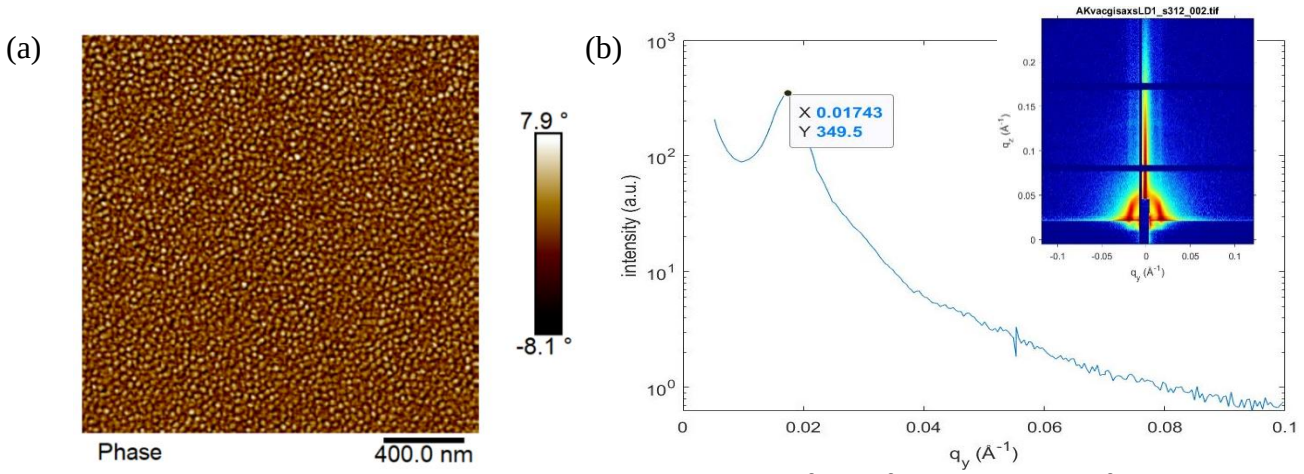

Figure 17: (a) AFM scan image and (b) In-plane scattering profiles of horizontal cut of inset 2D GISAXS pattern of 2wt% IL in 2% PS-*b*-PMMA(55K-22K).

As cast 100 nm 2% PS-*b*-PMMA(55K-22K) film with 2wt% IL started to show clear phase separation. The AFM phase image and the GISAXS pattern explained that. The calculated domain spacing from the q^* of first order peak of in-plane scattering profile was 36 nm.

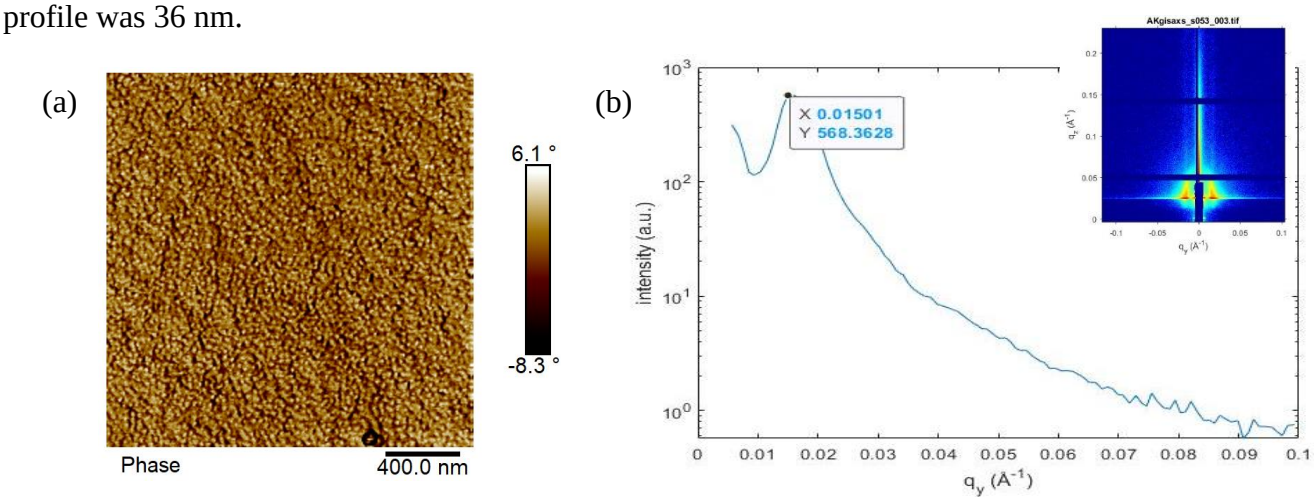

Figure 18: (a) AFM scan image and (b) In-plane scattering profiles of horizontal cut of inset 2D GISAXS pattern of 4wt% IL in 2% PS-*b*-PMMA(55K-22K).

As cast 100 nm 2% PS-*b*-PMMA(55K-22K) film with 4wt% IL started to show better phase separation. The AFM phase image and the GISAXS pattern explained that. The calculated domain spacing from the q^* of first order peak of in-plane scattering profile was 41.9 nm.

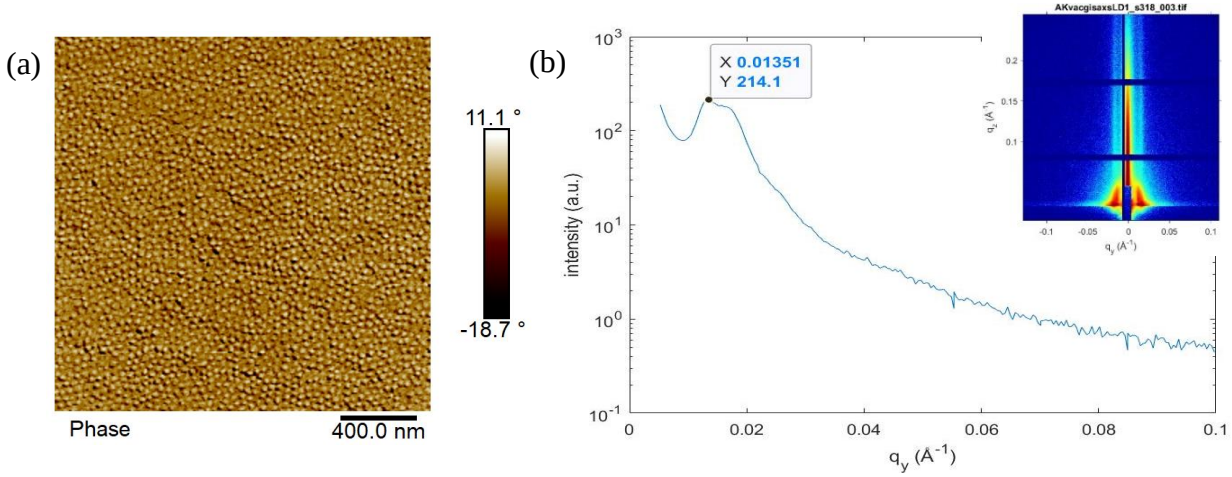

Figure 19: (a) AFM scan image and (b) In-plane scattering profiles of horizontal cut of inset 2D GISAXS pattern of 5wt% IL in 2% PS-*b*-PMMA(55K-22K).

As cast 100 nm 2% PS-*b*-PMMA(55K-22K) film with 5wt% IL showed clear phase separation. The AFM phase image and the GISAXS pattern supported that. The calculated domain spacing from the q^* of first order peak of in-plane scattering profile was 46.5 nm. The broadening of the peak might be due to heterogeneous domain spacing of vertical and parallel cylinders.

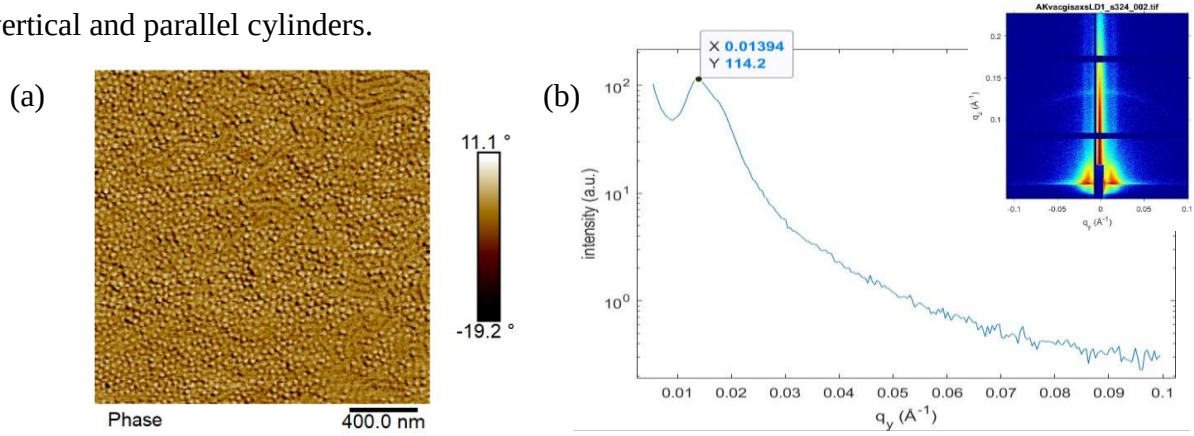

Figure 20: (a) AFM scan image and (b) In-plane scattering profiles of horizontal cut of inset 2D GISAXS pattern of 8wt% IL in 2% PS-*b*-PMMA(55K-22K).

As cast 100 nm 2% PS-*b*-PMMA(55K-22K) film with 8wt% IL showed clear phase separation and mixed orientation. The AFM phase image and the GISAXS pattern supported that. The calculated domain spacing from q^* of first order peak of the in-plane scattering profile was 45 nm. The broadening of the peak might be due to heterogeneous domain spacing.

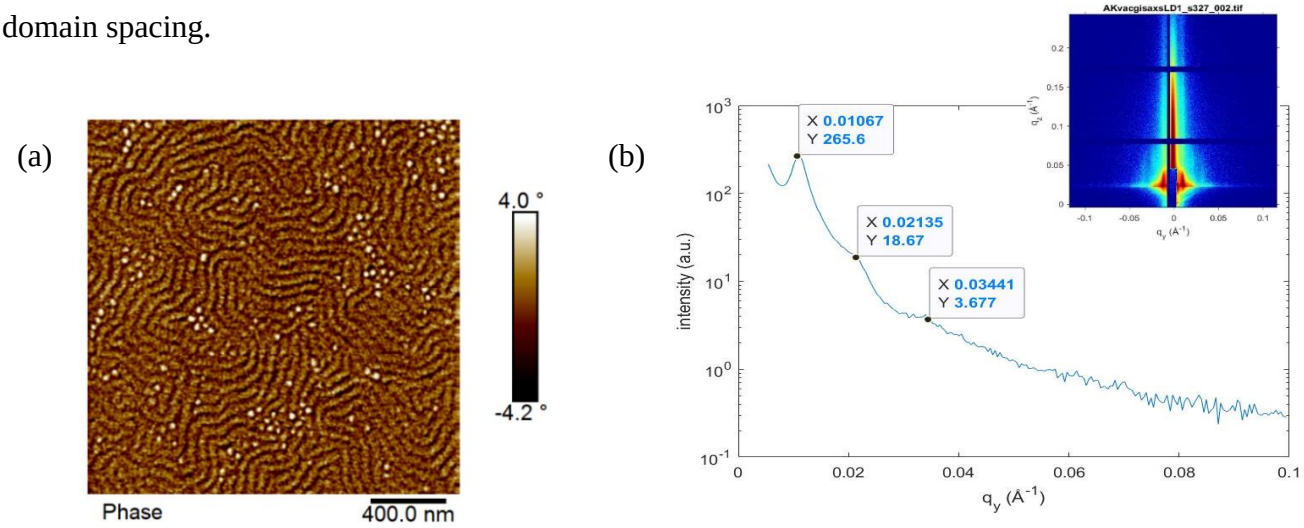

Figure 21: (a) AFM scan image and (b) In-plane scattering profiles of horizontal cut of inset 2D GISAXS pattern of 12wt% IL in 2% PS-*b*-PMMA(55K-22K).

As cast 100 nm 2% PS-*b*-PMMA(55K-22K) film with 12wt% IL showed clear phase separation but long-range ordering of in-plane parallel cylinders of PMMA on the surface. The AFM phase image and the GISAXS pattern explained the perpendicular-parallel mixed orientation. The calculated domain spacing from the q^* of each peak of in-plane scattering profile were 58.8 nm, 29.4 nm and 18.3 nm, respectively. The domain spacing did not follow a strict ratio of 3:2:1 but was close to a periodic value and indicative of parallel cylinders in the system.

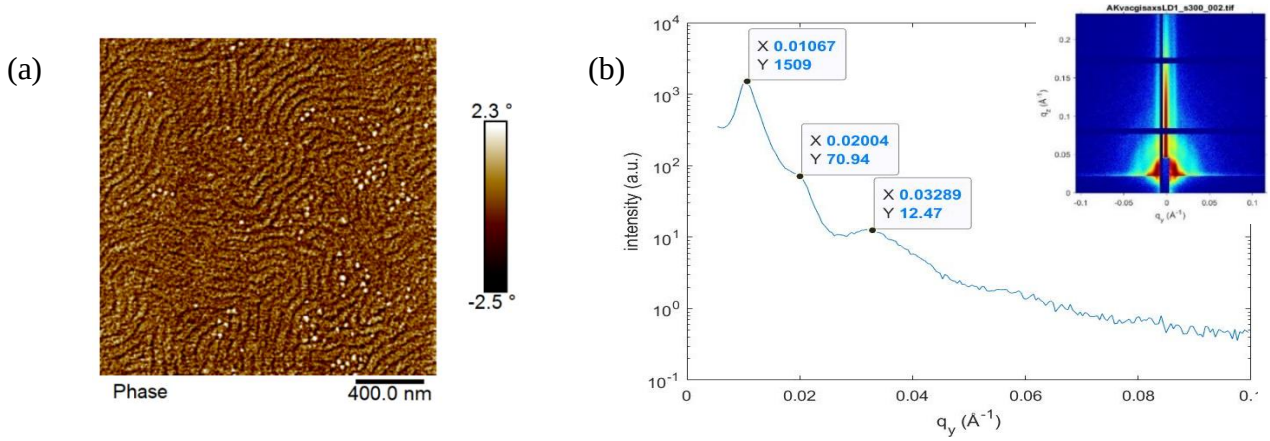

Figure 22: (a) AFM scan image and (b) In-plane scattering profiles of horizontal cut of inset 2D GISAXS pattern of 15wt% IL in 2% PS-*b*-PMMA(55K-22K).

As cast 100 nm 2% PS-*b*-PMMA(55K-22K) film with 15wt% IL showed more of meandering type orientation or parallel cylinders on the surface of the film. The AFM phase image and the GISAXS pattern explained the more parallel rather than perpendicular orientation. The calculated domain spacing from the q^* of each peak of in-plane scattering profile were 58.8 nm, 31.4 nm and 19.1 nm, respectively. The domain spacing did not follow a strict ratio of 3:2:1 but was close to the periodic value. The surface roughness was higher than other as cast films. It was indicative of parallel cylinders all through the thickness of the film.

The domain spacing value increased up to 5wt% IL uptake which indicated the swelling of PMMA cylinders by IL. At 8wt% IL addition the long-range ordering of parallel cylinders' orientation suppressed the domain spacing.

Table 1: Contact Angle (CA) measurement and Surface Energy(SE) calculation for 100 nm as cast film

100 nm as cast 2% PS-*b*-PMMA(55K-22K) with IL(wt%)	Water CA(°)	Diiodomethane CA(°)	SE (J/m^2)
Bare Si wafer	18.3	41.2	69.7
UV-ozone treated Si wafer	0.0	34.9	73.6
0% IL	45.9	30.8	58.2
2% IL	90.0	15.4	49.2
5% IL	44.2	15.1	61.9
8% IL	43.7	7.6	62.9
12% IL	90.6	32.5	43.2
15% IL	85.6	35.9	42.3

The surface energy measurement indicated that just like hydrophobic low energy polystyrene films, the BCP films also show low surface energy. Although the 5wt% and 8wt% IL added films showed high surface energy it might be due to some anomaly. There is some anomaly in the measurement of the surface energy as addition of IL goes to PMMA domain enhancing the phase segregation but changing surface energy

drastically.[7] So careful re-measurements of 2wt% IL to 8wt% IL added films are necessary.

As cast 100 nm 2% PS-*b*-PMMA(55K-22K) film with 12wt% IL clearly showed the most interesting orientation. To investigate further the film was dipped in methanol for 30 minutes to remove the IL and check change in orientation.

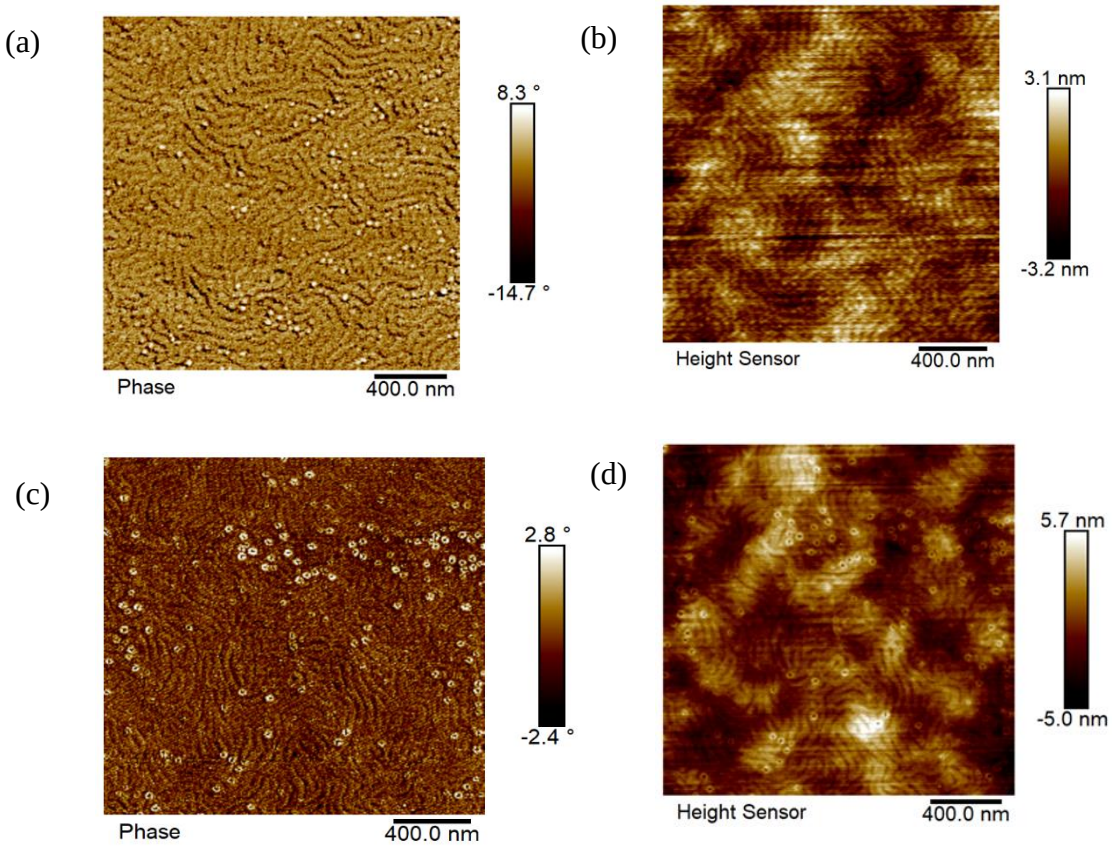

Figure 23: AFM scan image (a) phase and (b) height image of 12wt% IL 2% PS-*b*-PMMA(55K-22K) (c) phase and (d) height image of 12wt% IL in 2% PS-*b*-PMMA(55K-22K) after dipping in methanol for 30 minutes.

The phase image of the film after 30 minutes showed swollen perpendicular cylinder with open pores. The height image of the film before and after dipping showed the extent of long-range ordering of in-plane parallel cylinders all through the thickness of the film. The swollen cylinders might be indication of ionic liquid depletion.

Ablation Test

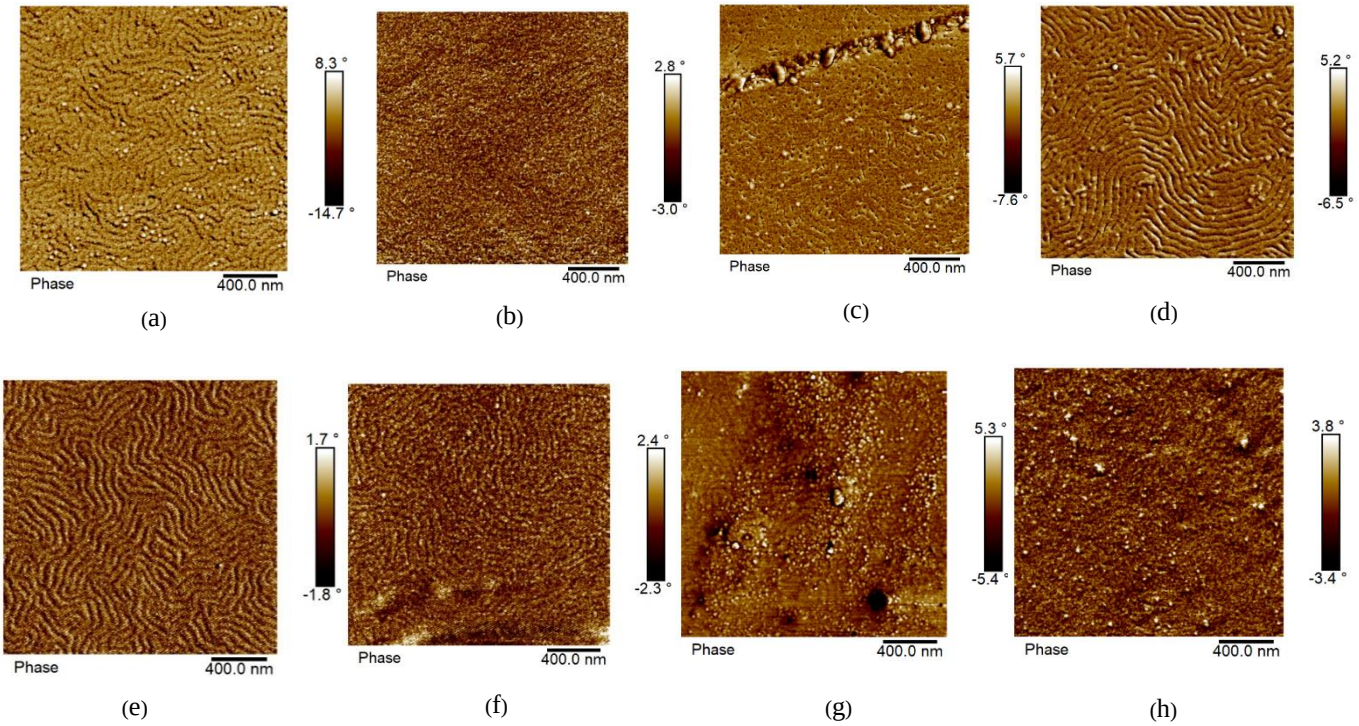

Figure 24: AFM scan image of 12wt% IL in 2% PS-*b*-PMMA(55K-22K) at (a) 100 nm, then UV-ozone etched for (b) 5 min at 91 nm (c) 10 min at 87.50 nm (d) 15 min at 80 nm (e) 20 min at 72 nm (f) 25 min at 63.5 nm (g) 30 min at 54. 6 nm and (h) 35 min at 45.6 nm.

To further check the meandering orientation of the as cast 100 nm 2% PS-*b*-PMMA(55K-22K) film with 12wt% IL it was systematically etched in UV-ozone chamber. The etching experiment was named ablation test and the thickness of the film was measured every 5 minute. From **Figure 24** from AFM phase image after etching down to 72 nm, the orientation stared to fade. So it is understood that the meandering is a surface phenomenon and the orientation was not all through the thickness.

After careful study of 100 nm thickness as cast films based on the phase separation and probable orientation, three more thickness i.e., 40 nm, 200 nm and 400 nm with four particular percentage of IL i.e., 0, 4, 8 and 12 were studied to get a better understanding of ordering of PMMA cylinders through variable thickness.

Film Thickness Variation

Film thickness: 40 nm

IL (wt%): 0%, 4%, 8%, 12%

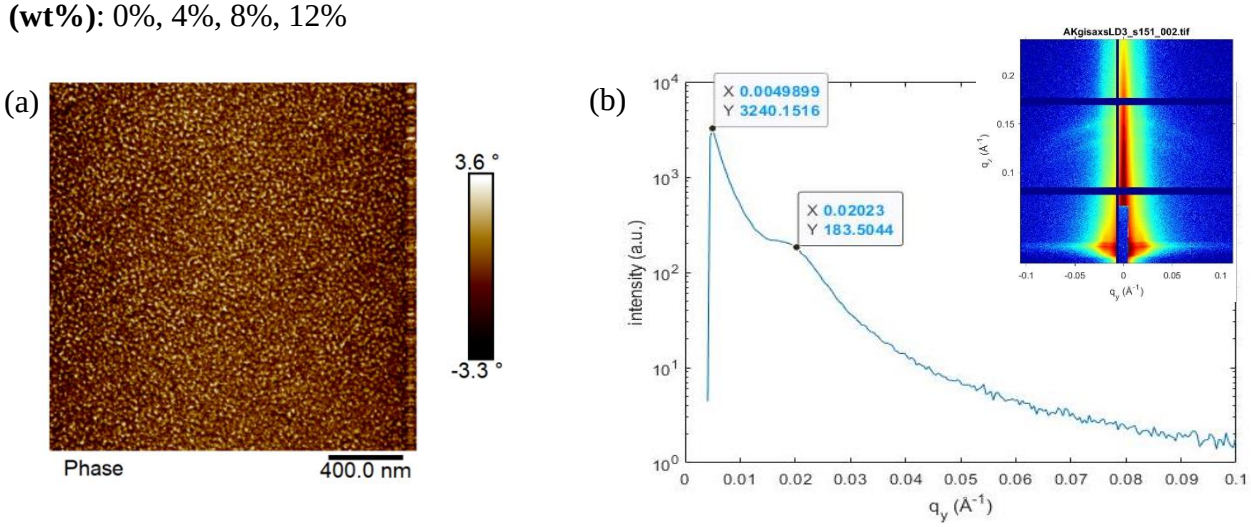

Figure 25: (a) AFM scan image and (b) In-plane scattering profiles of horizontal cut of inset 2D GISAXS pattern of 0wt% IL in 2% PS-*b*-PMMA(55K-22K) at 40 nm thickness.

As cast 40 nm 2% PS-*b*-PMMA(55K-22K) film without any IL showed no orientation. The AFM phase image and the GISAXS pattern explained that. The calculated domain spacing from the q^* of first order peak of in-plane scattering profile was 31.4 nm.

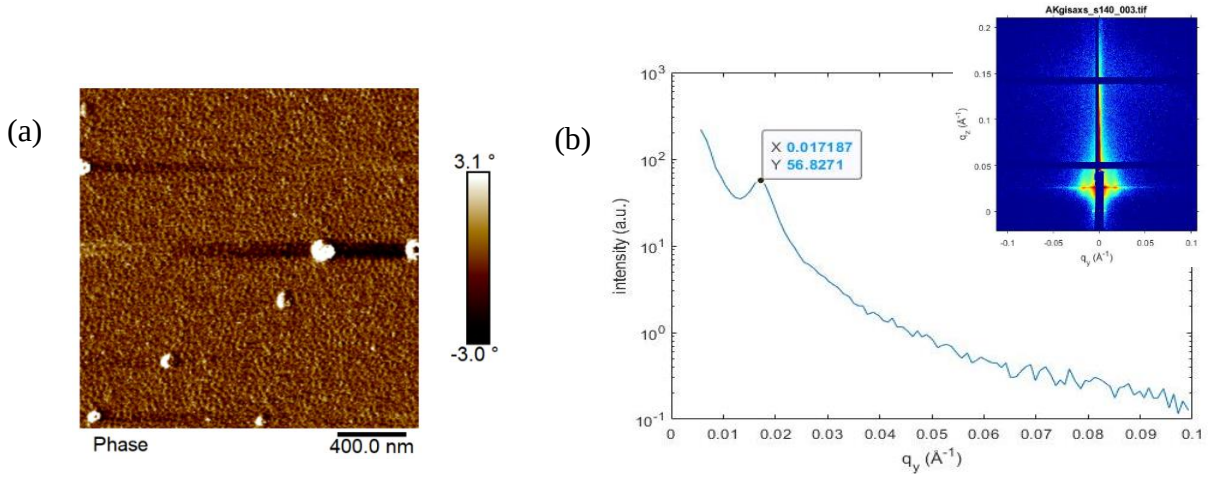

Figure 26: (a) AFM scan image and (b) In-plane scattering profiles of horizontal cut of inset 2D GISAXS pattern of 4wt% IL in 2% PS-*b*-PMMA(55K-22K) at 40 nm thickness.

As cast 40 nm 2% PS-*b*-PMMA(55K-22K) film with 4wt% IL showed no sign of orientation with lots of surface defects. The AFM phase image and the GISAXS pattern explained that. The calculated domain spacing from the q^* of first order peak of in-plane scattering profile was 36.6 nm.

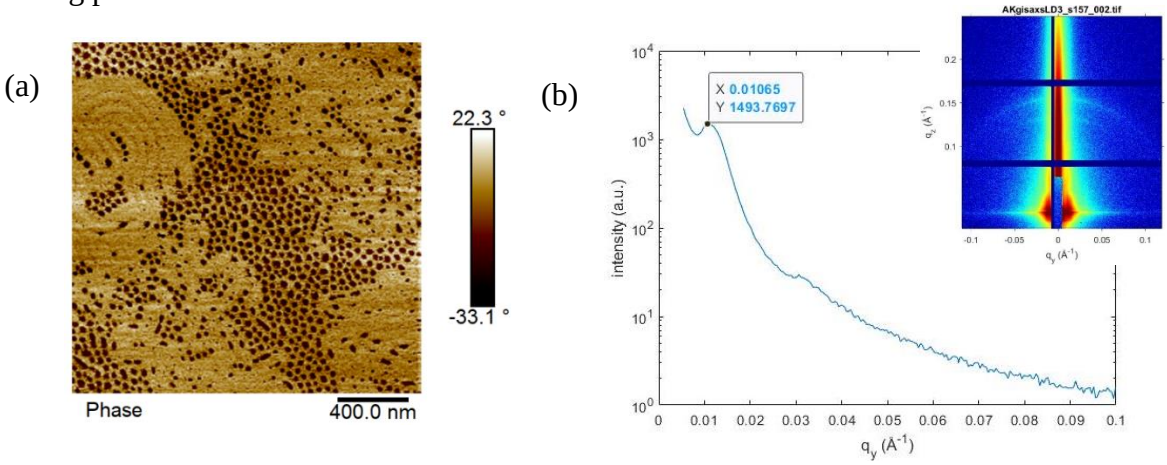

Figure 27: (a) AFM scan image and (b) In-plane scattering profiles of horizontal cut of inset 2D GISAXS pattern of 8wt% IL in 2% PS-*b*-PMMA(55K-22K) at 40 nm thickness.

As cast 40 nm 2% PS-*b*-PMMA(55K-22K) film with 8wt% IL showed perpendicular cylinder orientation but not uniformly and the PMMA cylinders were swollen. The AFM phase image and the GISAXS pattern supported that. The calculated domain spacing from the q^* of first order peak of in-plane scattering profile was 59 nm.

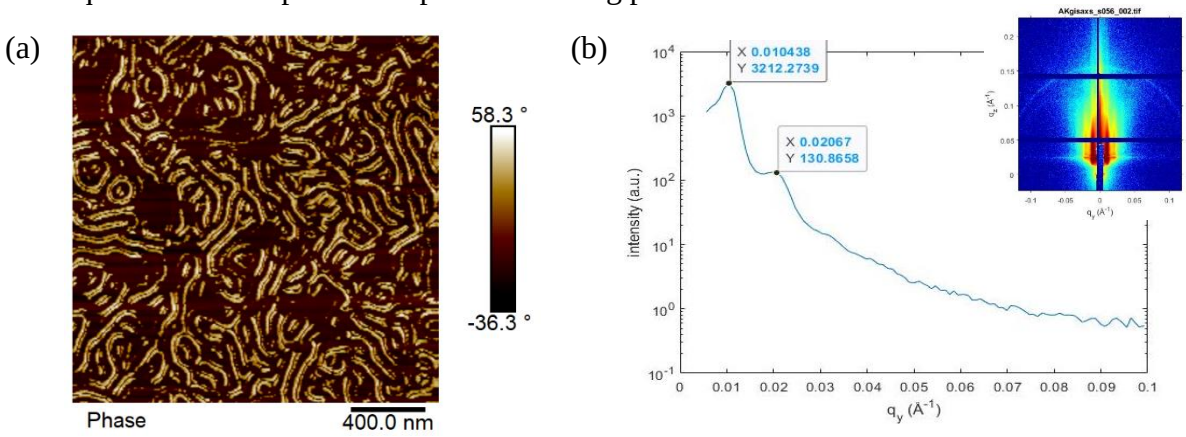

Figure 28: (a) AFM scan image and (b) In-plane scattering profiles of horizontal cut o inset 2D GISAXS pattern of 12wt% IL 2% PS-*b*-PMMA(55K-22K) at 40 nm thickness.

As cast 40 nm 2% PS-*b*-PMMA(55K-22K) film with 12wt% IL showed almost no perpendicular cylinder orientation. The AFM phase image and the GISAXS pattern supported the long-range ordering of in-plane parallel cylinders. The calculated domain spacing from the q^* of first order and higher peak of in-plane scattering profile was 60.4 nm and 30.3 nm indicative of periodicity, which might occur due to meandering of cylinders or parallel cylinders.

Compared to 100 nm as films the 40 nm films didn't show clear phase separation or distinct orientation. In thinner films the whole melt could be under stressor suppression which prohibits ordered orientation.[20]

Film thickness: 200 nm

IL (wt%): 0%, 4%, 8%, 12%

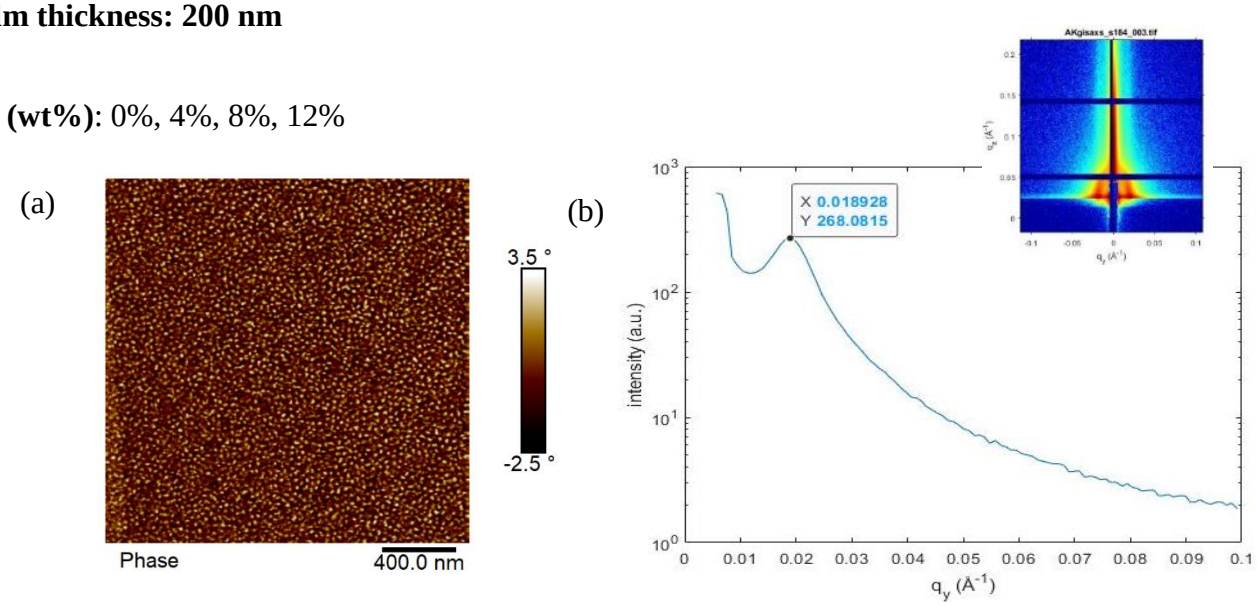

Figure 29: (a) AFM scan image and (b) In-plane scattering profiles of horizontal cut of inset 2D GISAXS pattern of 0wt% IL in 2% PS-*b*-PMMA(55K-22K) at 200 nm thickness.

As cast 200 nm 2% PS-*b*-PMMA(55K-22K) film without any IL showed no orientation. The AFM phase image and the GISAXS pattern explained that. The calculated domain spacing from the q^* of first order peak of in-plane scattering profile was 33.2 nm.

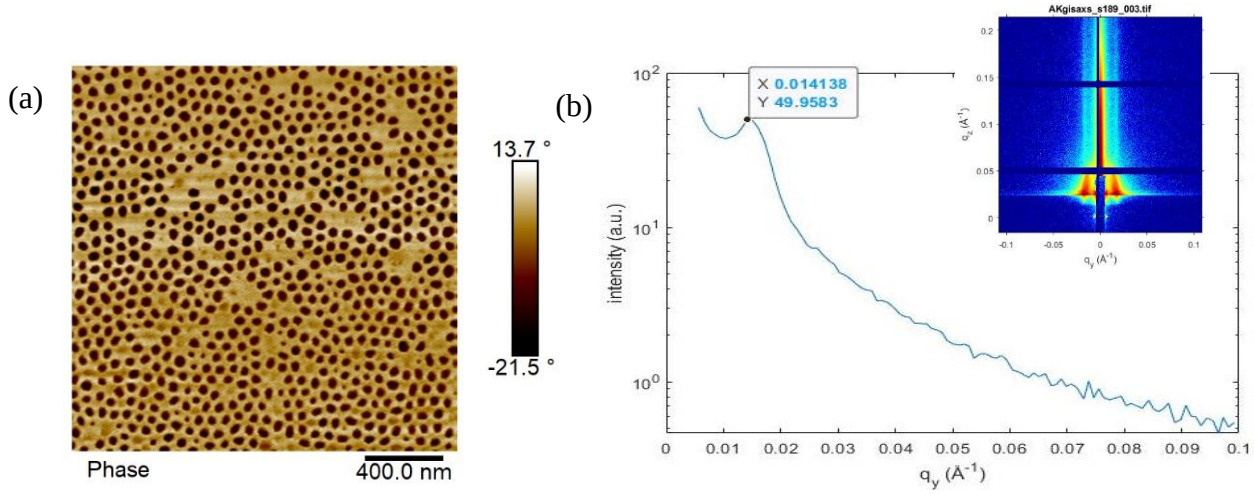

Figure 30: (a) AFM scan image and (b) In-plane scattering profiles of horizontal cut of inset 2D GISAXS pattern of 4wt% IL in 2% PS-*b*-PMMA(55K-22K) at 200 nm thickness.

As cast 200 nm 2% PS-*b*-PMMA(55K-22K) film with 4wt% IL showed preferred perpendicular ordered cylinder orientation. The vertical perpendicular cylinders are not ordered uniformly throughout the film. The AFM phase image and the GISAXS pattern explained this orientation. The calculated domain spacing from the q^* of first order peak of in-plane scattering profile was 44.4 nm.

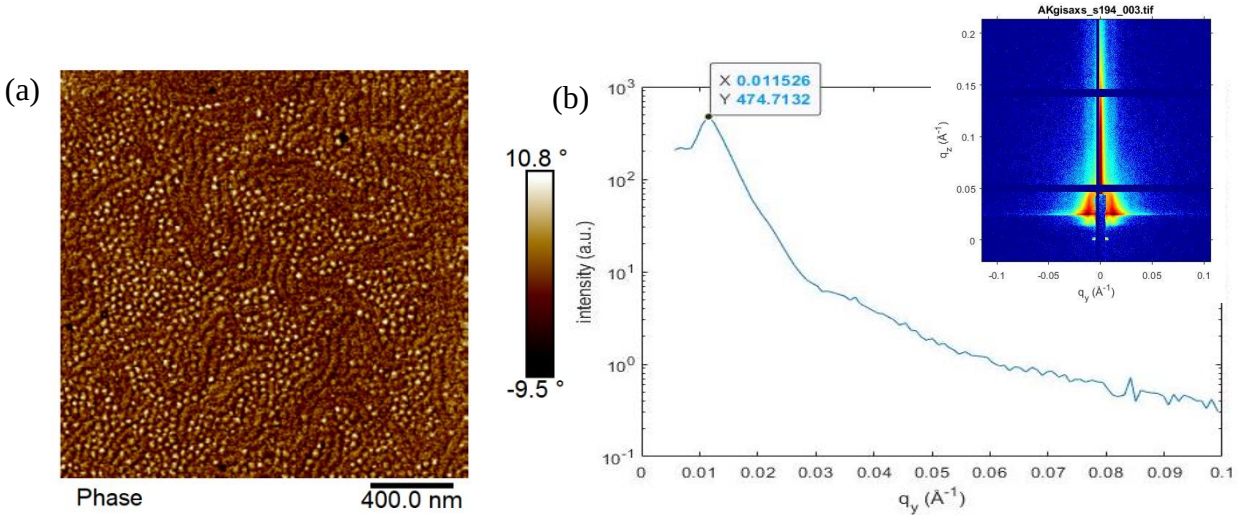

Figure 31: (a) AFM scan image and (b) In-plane scattering profiles of horizontal cut of inset 2D GISAXS pattern of 8wt% IL in 2% PS-*b*-PMMA(55K-22K) at 200 nm thickness.

As cast 200 nm 2% PS-*b*-PMMA(55K-22K) film with 8wt% IL showed clear phase separation with orientation of in-plane parallel cylinders. The AFM phase image and the

GISAXS pattern supported the mixed or more accurately meandering chain orientation. The calculated domain spacing from the q^* of first order peak of in-plane scattering profile was 54.6 nm.

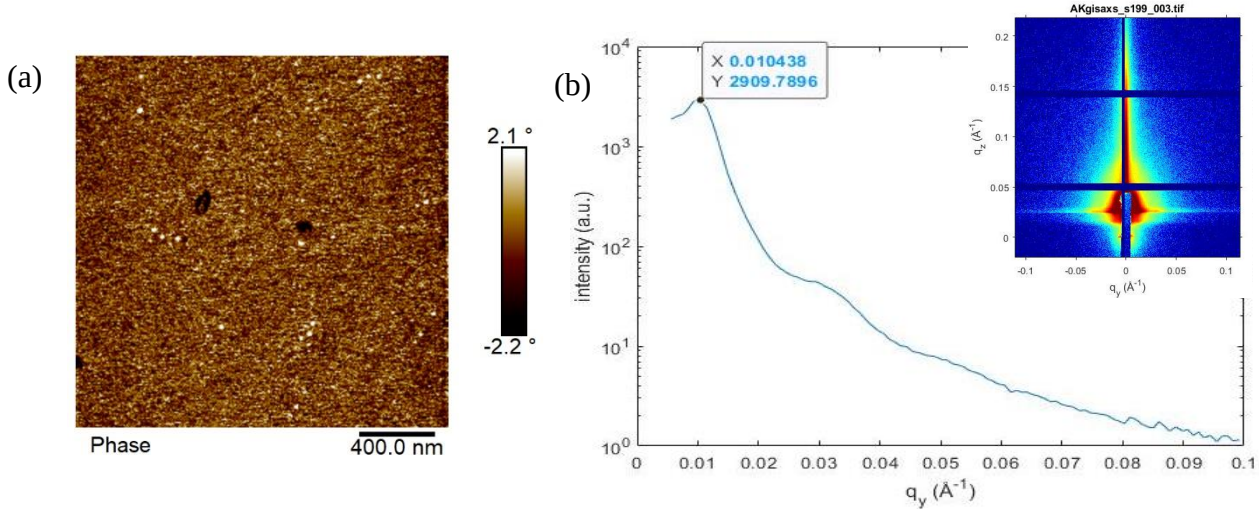

Figure 32: (a) AFM scan image and (b) In-plane scattering profiles of horizontal cut of inset 2D GISAXS pattern of 12wt% IL in 2% PS-*b*-PMMA(55K-22K) at 200 nm thickness.

As cast 200 nm 2% PS-*b*-PMMA(55K-22K) film with 12wt% IL showed no clear phase separation or orientation. The AFM phase image and the GISAXS pattern supported the loss of chain orientation. The calculated domain spacing from the q^* of first order peak of in-plane scattering profile was 60.2 nm. There was rise of higher order peaks with very low intensity.

With increased thickness the orientation of the PMMA cylinders were prominent up to 8wt% IL addition but with 12wt% IL addition the ordering was not throughout the film thickness. The roughness also increased with increasing values of domain spacing.

Film thickness: 400 nm

IL (wt%): 0%, 4%, 8%, 12%

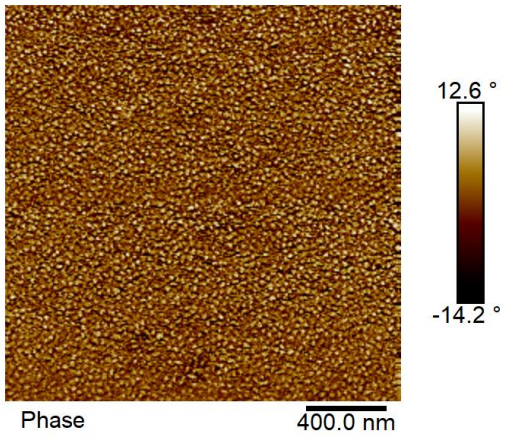

Figure 33: AFM scan image of 0wt% IL in 2% PS-*b*-PMMA(55K-22K) at 400 nm Thickness.

The AFM phase image of as cast 400 nm 2% PS-*b*-PMMA(55K-22K) film without any IL showed no clear phase separation.

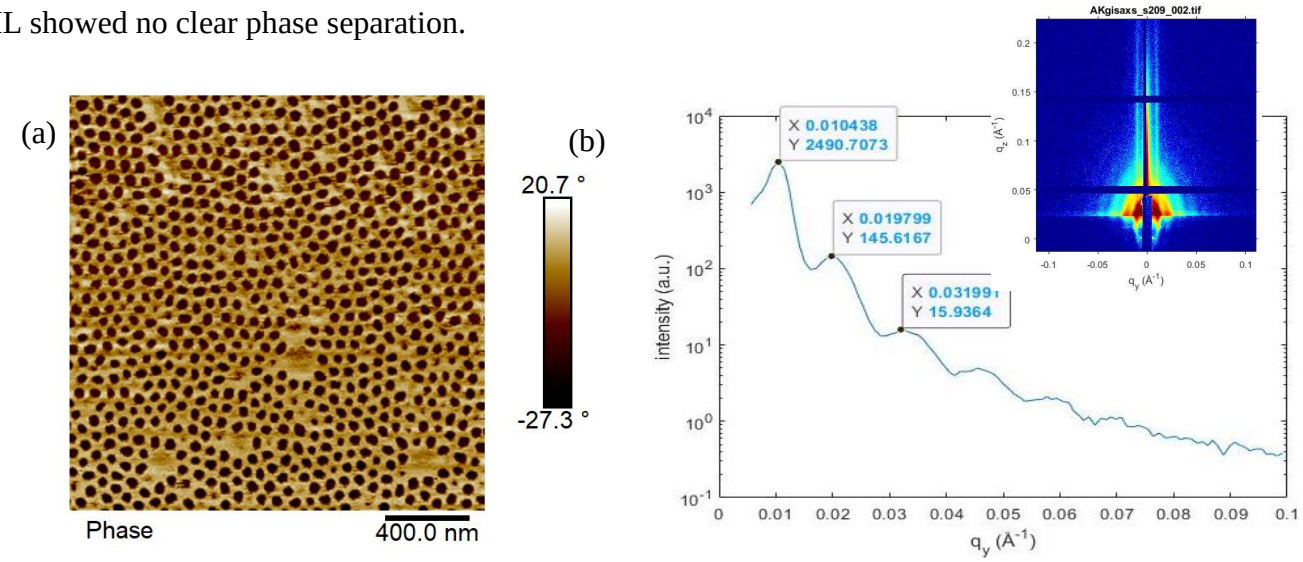

Figure 34: (a) AFM scan image and (b) In-plane scattering profiles of horizontal cut of inset 2D GISAXS pattern of 4wt% IL in 2% PS-*b*-PMMA(55K-22K) at 400 nm thickness.

As cast 400 nm 2% PS-*b*-PMMA(55K-22K) film with 4wt% IL showed clear phase separation and preferred perpendicular cylinder orientation. The vertical perpendicular cylinders were not ordered uniformly throughout the film. The AFM phase image and the

GISAXS pattern explained the perpendicular orientation. The calculated domain spacing from the q^* of each peak of in-plane scattering profile were 60.2 nm, 31.7 nm and 19.6 nm. The domain spacing did not follow a strict ratio of 3:2:1 but was close to a periodic value indicative of parallel cylinders through the thickness of the film.

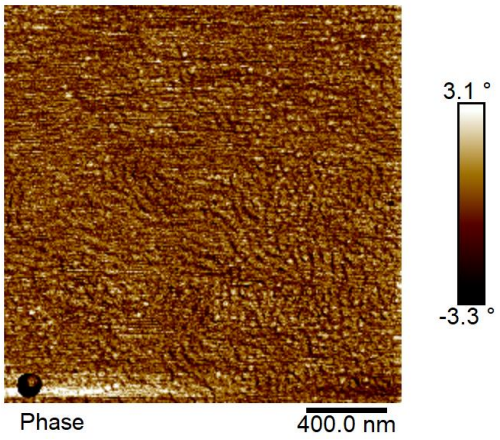

Figure 35: AFM scan image of 8wt% IL in 2% PS-*b*-PMMA(55K-22K) at 400 nm thickness.

The AFM phase image of as cast 400 nm 2% PS-*b*-PMMA(55K-22K) film with 8wt% IL showed no clear phase separation. From the phase image it seemed the orientation was of long-range in-plane parallel cylinders on the surface of the film was quite rough.

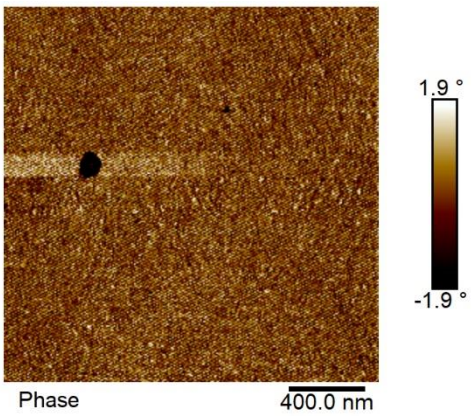

Figure 36: AFM scan image of 12wt% IL in 2% PS-*b*-PMMA(55K-22K) at 400 nm thickness.

The AFM phase image of as cast 400 nm 2% PS-*b*-PMMA(55K-22K) film with 12wt% IL showed almost no phase separation. From the phase image it seemed the orientation is completely parallel and the surface of the film was quite rough.

Table 2: Contact Angle (CA) measurement and Surface Energy(SE) calculation for 400 nm as cast film

400 nm as cast 2% PS-*b*-PMMA(55K-22K) with IL(wt%)	Water CA(°)	Diiodomethane CA(°)	SE (J/m^2)
Bare Si wafer	18.3	41.2	69.7
UV-ozone treated Si wafer	0.0	34.9	73.6
0% IL	85.9	31.5	46.2
4% IL	85.2	18.0	48.4
8% IL	86.6	18.0	48.3
12% IL	82.9	22.7	47.1

The surface energy measurement indicated that just like hydrophobic low energy polystyrene films, the BCP films also show low surface energy. Lower surface energy indicated lower wettability. The films with or without IL showed surface energy in a close range supporting the literature.[7]

As cast 400 nm 2% PS-*b*-PMMA(55K-22K) film with 4wt% IL clearly showed the most interesting orientation. To investigate further the film was dipped in methanol for 30 minutes to remove the IL and check change in orientation.

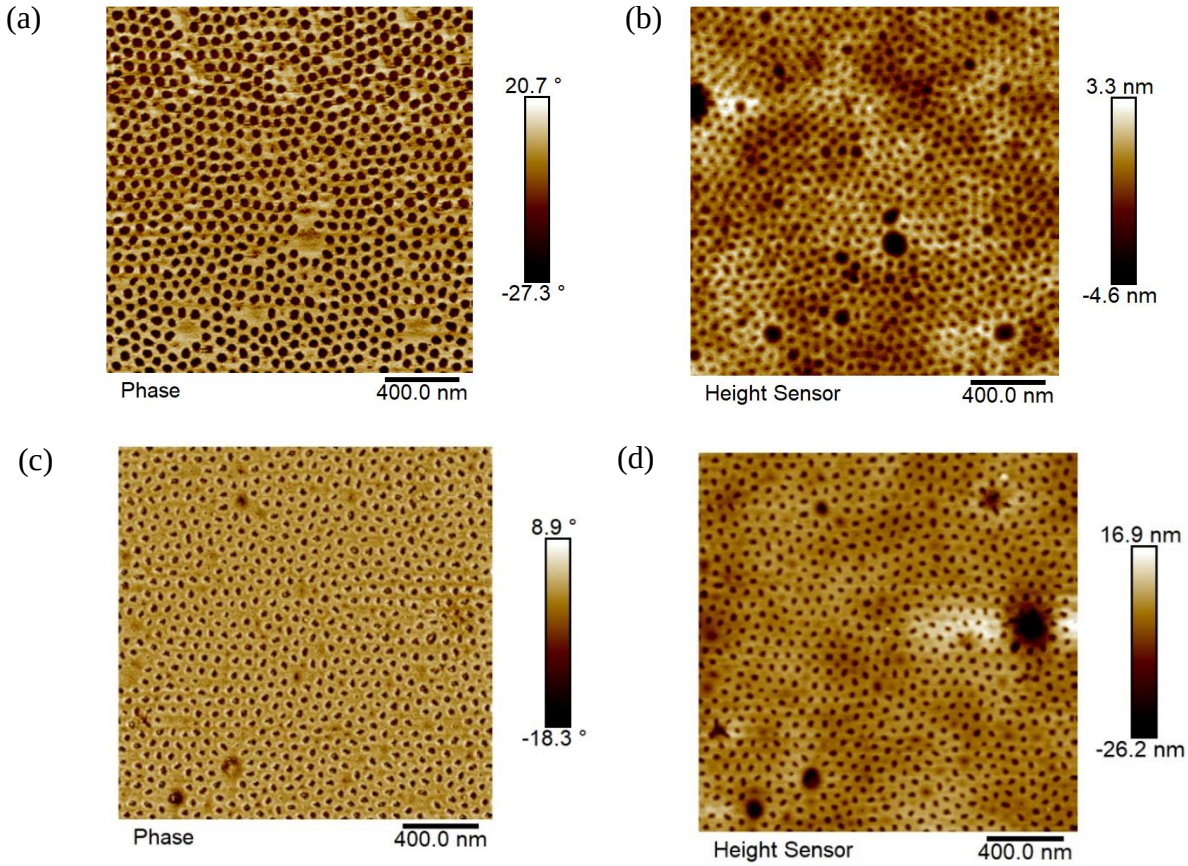

Figure 37: AFM scan image (a) phase and (b) height image of 400 nm thick 4wt% IL in 2% PS-*b*-PMMA(55K-22K) (c) phase and (d) height image of 400 nm thick 4wt% IL in 2% PS-*b*-PMMA(55K-22K) after dipping in methanol for 30 minutes.

The phase image of the film after 30 minutes showed swollen perpendicular cylinder with open pores. The height image of the film before and after dipping showed the extent of the preferred orientation. The swollen cylinders might be indication of ionic liquid leaching out.

Ablation Test:

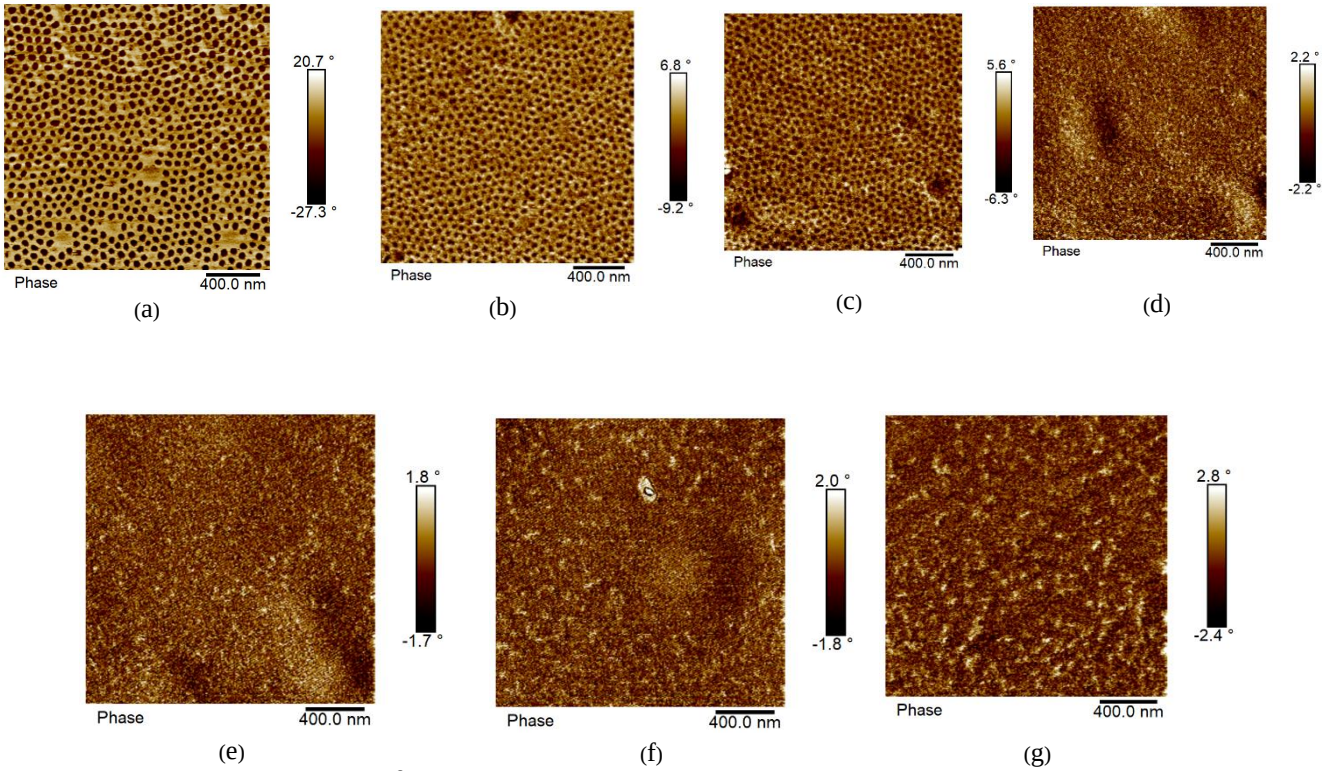

Figure 38: AFM scan image of 4wt% IL in 2% PS-*b*-PMMA(55K-22K) at (a) 400 nm, then UV-ozone etched for (b) 5 min at 385 nm (c) 10 min at 373 nm (d) 15 min at 350.5 nm (e) 20 min at 339.6 nm (f) 25 min at 324.6 nm and (g) 30 min at 296.8 nm.

To further check the perpendicular orientation of the as cast 400 nm 2% PS-*b*-PMMA(55K-22K) film with 4wt% IL it was systematically etched in UV-ozone chamber. The etching experiment was named ablation test and the thickness of the film was measured every 5 minute. From **Figure 24** from AFM phase image after etching down to approximately 300 nm, the orientation stared to disappear. So it is understood that the ordering is a surface phenomenon and the orientation was not all through the thickness.

Direct Immersion Annealed (DIA) Films

After careful study of as cast films based on the phase separation and probable orientation of all four thickness i.e., 40 nm, 100 nm, 200 nm and 400 nm, the films were subjected to study effect of DIA. A solvent mixture was designed to induce ordering without de-wetting the films. Solvent environment dictates the formation of ordering. Hansen solubility parameters of solvents were used to check the compatibility among the solvents and to check the miscibility of the solvents.[21]

Table 3: Hansen solubility parameter values

Solvent/Polymer	δ_D	δ_P	δ_H	δ_T
Toluene	18.0	1.4	2.0	18.2
Heptane	15.3	0	0	15.3
Polystyrene (PS)	18.5	4.5	2.9	19.2
Poly(methyl methacrylate) (PMMA)	18.6	10.5	5.1	22.0

Toluene was the good solvent which in small fraction regulated the mobility of the polymer chains and heptane was the poor solvent in larger fraction maintained the rate of dissolution of the film.[3]

The experiment was first done with 100 nm thick films. The films were immersed in the DIA mixture for certain time to test the desired orientation. Then AFM scan and GISAXS scattering pattern confirmed the orientation.

Film thickness: 100 nm

IL (wt%): 0%, 2%, 4%, 5%, 8%, 12% in 2% PS-*b*-PMMA (55K-22K)

DIA solvent mixture – Toluene: Heptane= 1:3 for 30 minutes

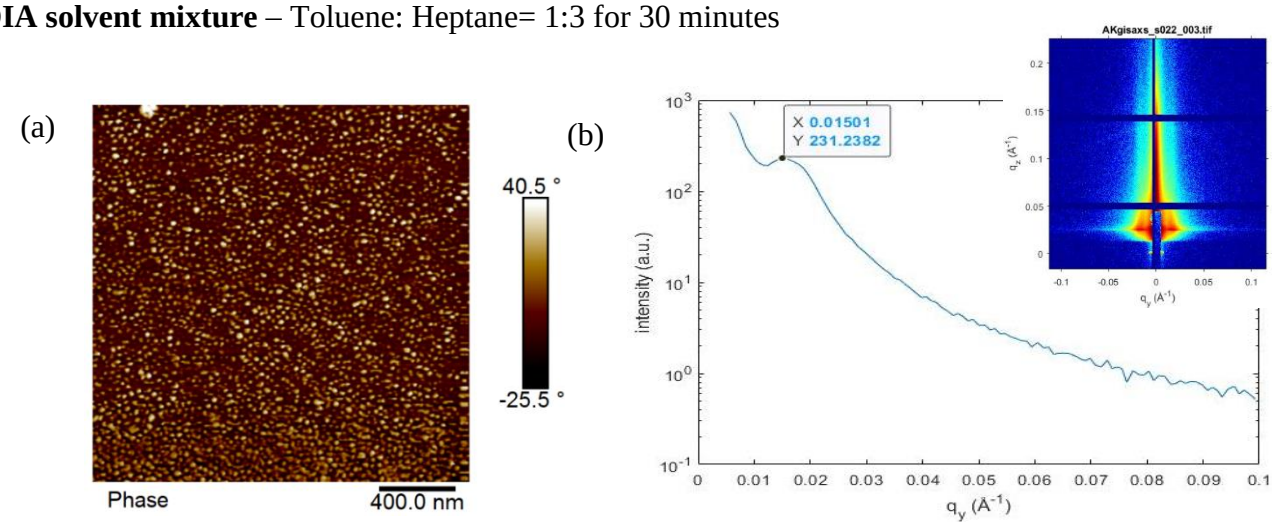

Figure 39: (a) AFM scan image and (b) In-plane scattering profiles of horizontal cut of inset 2D GISAXS pattern of 0wt% IL in 2% PS-*b*-PMMA(55K-22K) DIA film at 100 nm thickness.

DIA 100 nm 2% PS-*b*-PMMA(55K-22K) film without any IL showed no prominent orientation or phase separation supported by AFM phase image and GISAXS scattering pattern. The in-plane scattering profile gave domain spacing of 41.9 nm from the q^* of the first order peak.

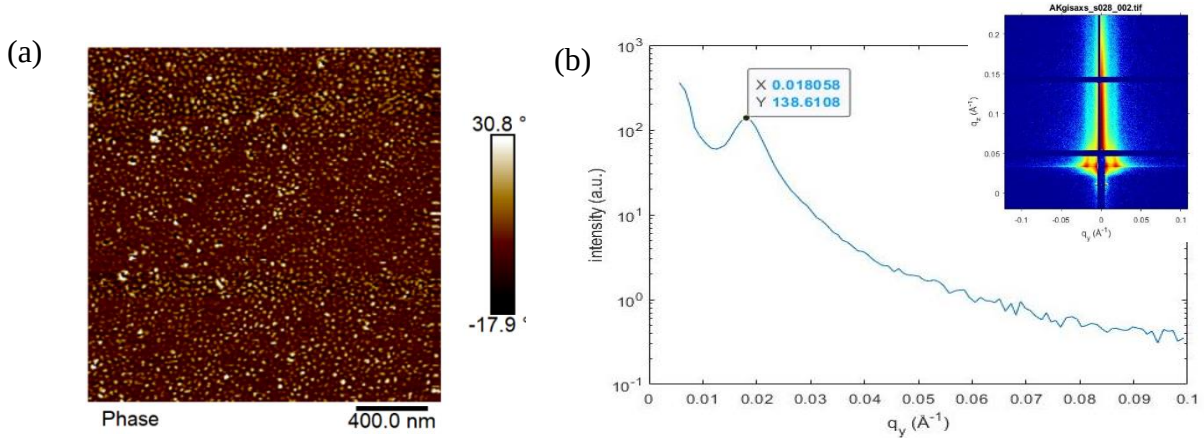

Figure 40: (a) AFM scan image and (b) In-plane scattering profiles of horizontal cut of inset 2D GISAXS pattern of 2wt% IL in 2% PS-*b*-PMMA(55K-22K) DIA film at 100 nm thickness.

DIA 100 nm 2% PS-*b*-PMMA(55K-22K) film with 2wt% IL showed no prominent orientation and it was supported by AFM phase image and GISAXS scattering pattern. The in-plane scattering profile gave domain spacing of 34.8 nm from the q^* of the first order peak.

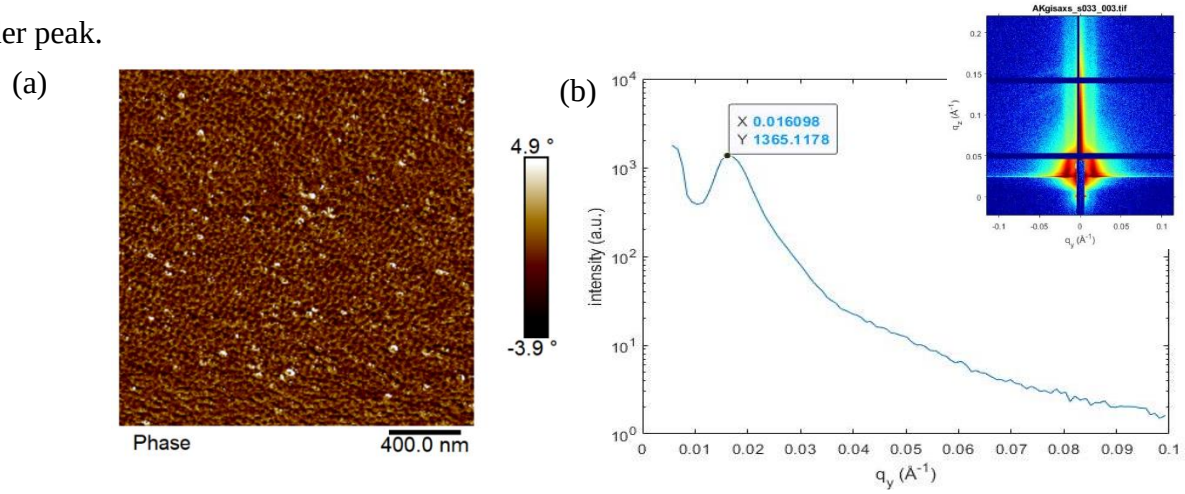

Figure 41: (a) AFM scan image and (b) In-plane scattering profiles of horizontal cut of inset 2D GISAXS pattern of 4wt% IL in 2% PS-*b*-PMMA(55K-22K) DIA film at 100 nm thickness.

DIA 100 nm 2% PS-*b*-PMMA(55K-22K) film with 4wt% IL showed perpendicular orientation to some extent and it was supported by AFM phase image and GISAXS scattering pattern. The film had quite a number of defects. The in-plane scattering profile gave domain spacing of 39.3 nm from the q^* of the first order peak.

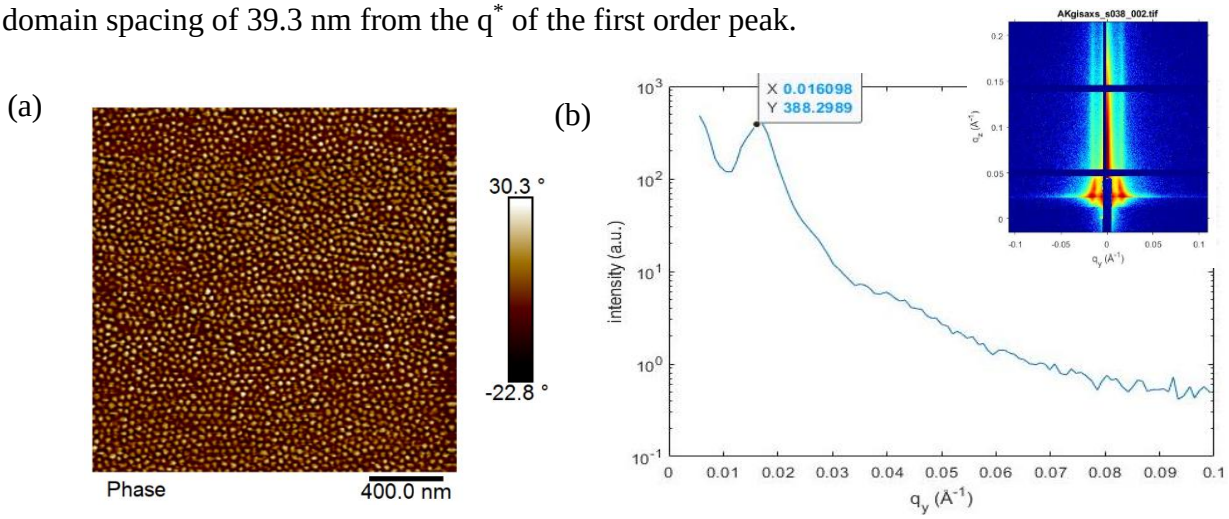

Figure 42: (a) AFM scan image and (b) In-plane scattering profiles of horizontal cut of inset 2D GISAXS pattern of 5wt% IL in 2% PS-*b*-PMMA(55K-22K) DIA film at 100 nm thickness.

DIA 100 nm 2% PS-*b*-PMMA(55K-22K) film with 5wt% IL showed better perpendicular orientation and phase separation compared to the previous film. It was supported by AFM phase image and GISAXS scattering pattern. The in-plane scattering profile gave domain spacing of 39.0 nm from the q^* of the first order peak.

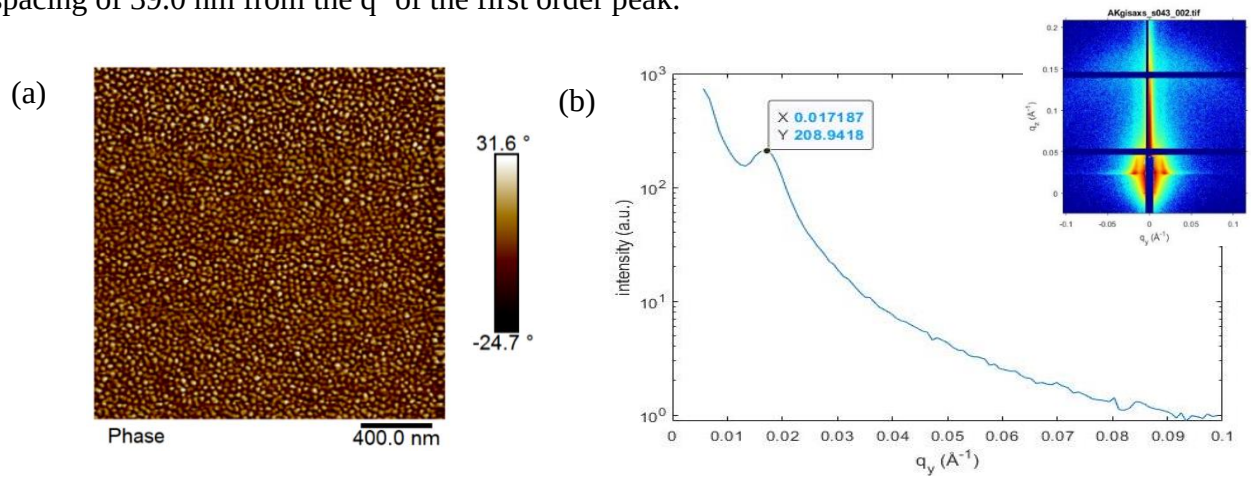

Figure 43: (a) AFM scan image and (b) In-plane scattering profiles of horizontal cut of inset 2D GISAXS pattern of 8wt% IL in 2% PS-*b*-PMMA(55K-22K) DIA film at 100 nm thickness.

DIA 100 nm 2% PS-*b*-PMMA(55K-22K) film with 8wt% IL showed clear phase separation and perpendicular orientation at some extent compared to the previous film. It was supported by AFM phase image and GISAXS scattering pattern. The in-plane scattering profile gave domain spacing of 36.5 nm from the q^* of the first order peak.

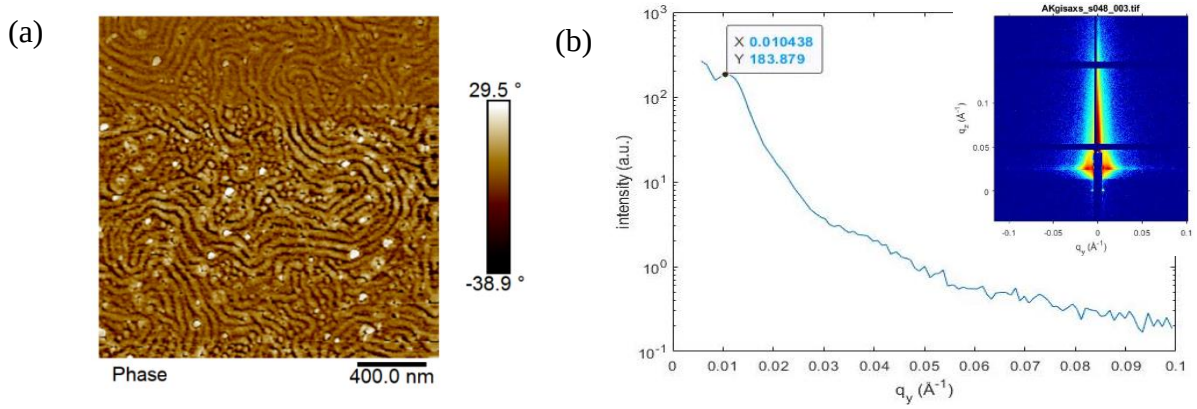

Figure 44: (a) AFM scan image and (b) In-plane scattering profiles of horizontal cut of inset 2D GISAXS pattern of 12wt% IL in 2% PS-*b*-PMMA(55K-22K) DIA film at 100 nm thickness.

DIA 100 nm 2% PS-*b*-PMMA(55K-22K) film with 12wt% IL showed clear phase separation but in-plane long-range ordering of PMMA parallel cylinders on the surface. The meandering of the chains was clear in AFM phase image and GISAXS scattering pattern. The film had quite a number of defects, the cylindrical pores had opening and the roughness of the film was high. The in-plane scattering profile gave domain spacing of 60.4 nm from the q^* of the first order peak. The periodic ratio of the domain spacing of the as cast film had not been observed on the DIA film. The cylinders were swollen.

For a systematic study other DIA mixture ratio was studied for the 100 nm thick film. 12wt% IL in 2% PS-*b*-PMMA(55K-22K) film was chosen for this study. This film was annealed or immersed in DIA mixture of toluene: heptane = 1:3 ratios for 30 minutes. First study was for the same DIA solvent mixture but for longer time.

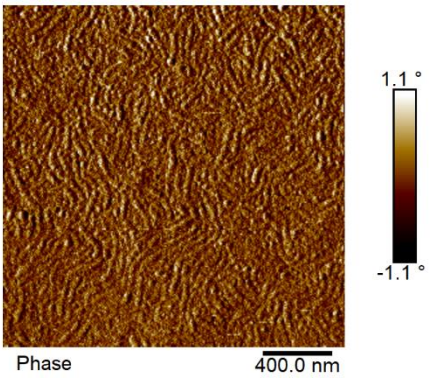

Figure 45: AFM scan image of 12wt% IL in 2% PS-*b*-PMMA(55K-22K) film of 100 nm thickness annealed in DIA mixture of toluene: heptane = 1:3 for 2 hours.

From the AFM scan of **Figure 45** it was evident that the 12wt% IL in 2% PS-*b*-PMMA(55K-22K) film of 100 nm thickness immersed in DIA solvent mixture of toluene: heptane = 1:3 for 2 hours instead of 30 minutes didn't improve the vertical orientation. The contrast of the phase image was not good because of difference in height.

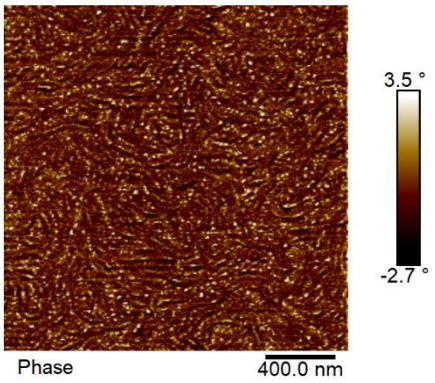

Figure 46: AFM scan image of 12wt% IL in 2% PS-*b*-PMMA(55K-22K) film of 100 nm thickness annealed in DIA mixture of toluene: heptane = 1:2 for 2 hours.

From the AFM scan of **Figure 46** showed that the 12wt% IL in 2% PS-*b*-PMMA(55K-22K) film of 100 nm thickness immersed in DIA solvent mixture of toluene: heptane = 1:2 for 2 hours didn't facilitate the orientation in that extant. It did show better phase separation and the parallel cylinders are oriented on the surface.

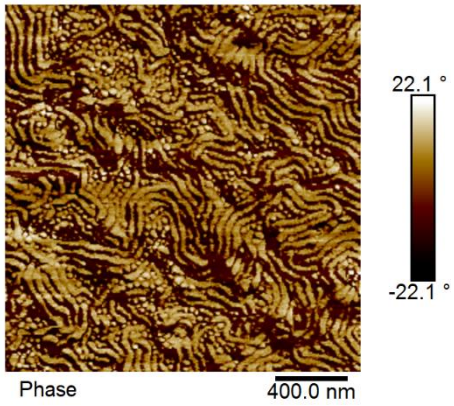

Figure 47: AFM scan image of 12wt% IL in 2% PS-*b*-PMMA(55K-22K) film of 100 nm thickness annealed in DIA mixture of toluene: heptane = 1:6 for 2 hours.

From the AFM scan of **Figure 47** showed that the 12wt% IL in 2% PS-*b*-PMMA(55K-22K) film of 100 nm thickness immersed in DIA solvent mixture of toluene: heptane = 1:6 for 2 hours didn't improve the orientation rather swelling the cylinders and oriented parallel on the surface.

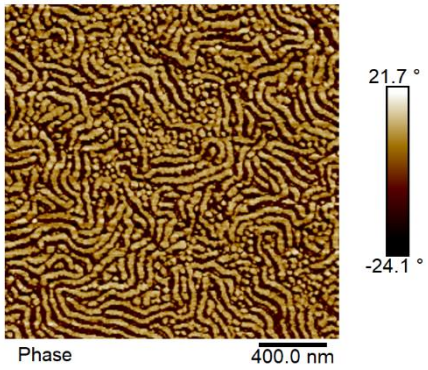

Figure 48: AFM scan image of 12wt% IL in 2% PS-*b*-PMMA(55K-22K) film of 100 nm thickness annealed in DIA mixture of toluene: heptane = 1:9 for 2 hours.

From the AFM scan of **Figure 48** showed that the 12wt% IL in 2% PS-*b*-PMMA(55K-22K) film of 100 nm thickness immersed in DIA solvent mixture of toluene: heptane = 1:9 for 2 hours didn't facilitate the desired orientation. The good solvent toluene was in a small amount which was the reason of the chains had enough mobility but not oriented in preferred manner. It did show good phase separation to some extent.

Film Thickness: 40 nm

IL (wt%): 0%, 4%, 8%, 12%

DIA solvent mixture – Toluene: Heptane= 1:3 for 30 minutes

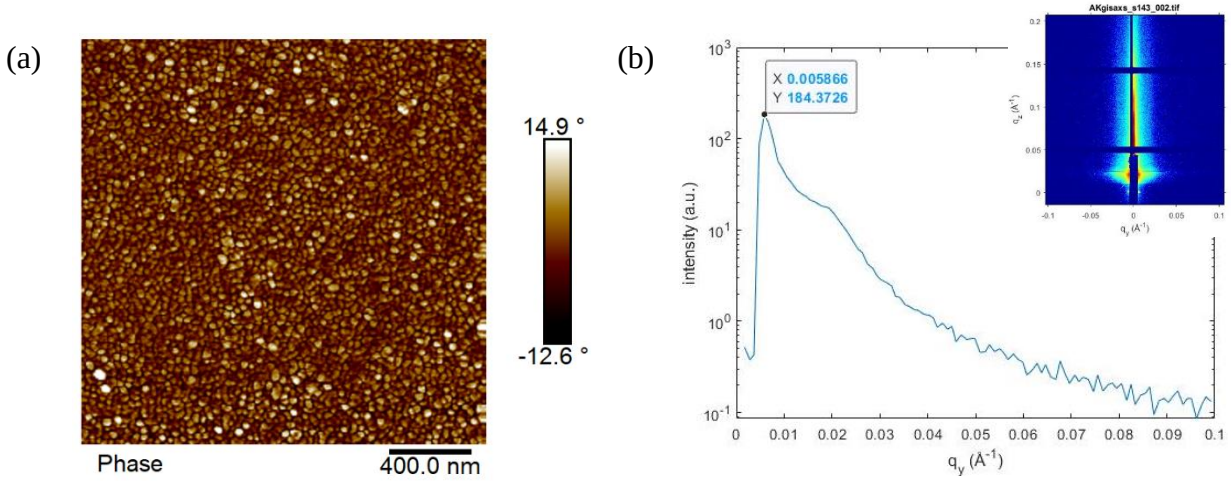

Figure 49: (a) AFM scan image and (b) In-plane scattering profiles of horizontal cut of inset 2D GISAXS pattern of 0wt% IL in 2% PS-*b*-PMMA(55K-22K) DIA film at 40 nm thickness.

DIA 40 nm 2% PS-*b*-PMMA(55K-22K) film without IL showed some phase separation but mixed orientation. The meandering of the chains was clear in AFM phase image and GISAXS scattering pattern. The in-plane scattering profile showed too small of a q_y value.

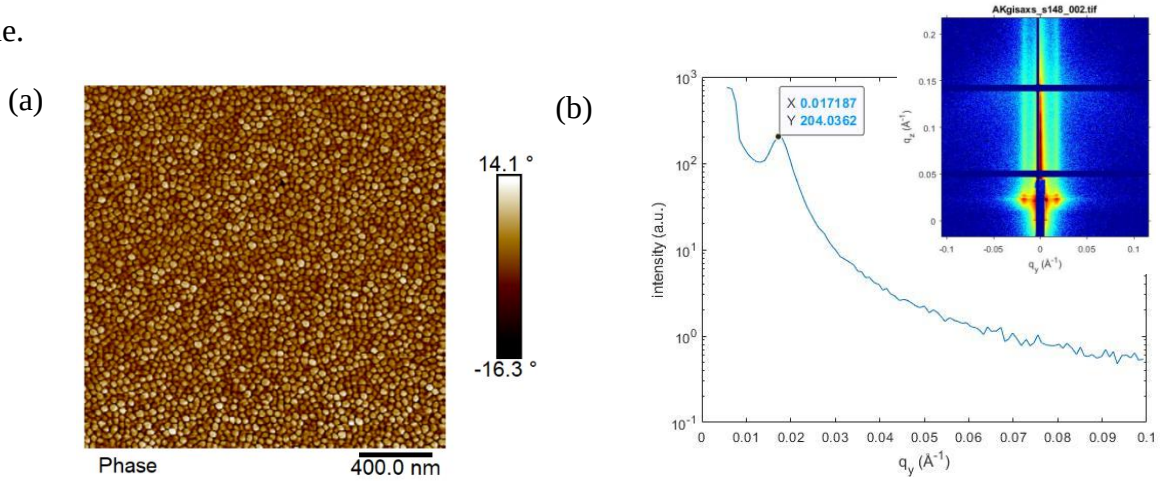

Figure 50: (a) AFM scan image and (b) In-plane scattering profiles of horizontal cut of inset 2D GISAXS pattern of 4wt% IL in 2% PS-*b*-PMMA(55K-22K) DIA film at 40 nm thickness.

DIA 40 nm 2% PS-*b*-PMMA(55K-22K) film with 4wt% IL showed some clear phase separation and some preferred vertical orientation. The meandering of the chains was not clear in AFM phase image and GISAXS scattering pattern. The cylinders were swollen and the in-plane scattering profile showed domain spacing of 36.5 nm from the q^* of the first order peak, smaller than as cast film.

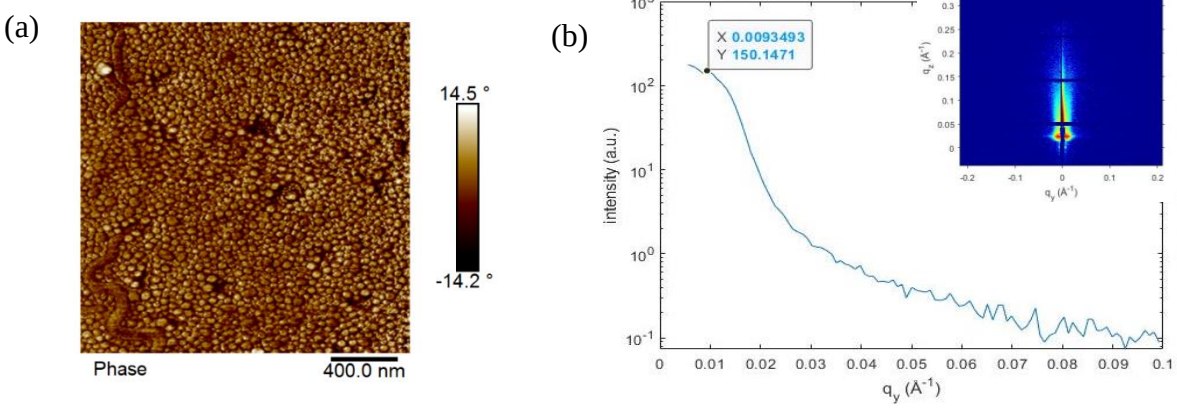

Figure 51: (a) AFM scan image and (b) In-plane scattering profiles of horizontal cut of inset 2D GISAXS pattern of 8wt% IL in 2% PS-*b*-PMMA(55K-22K) DIA film at 40 nm thickness.

DIA 40 nm 2% PS-*b*-PMMA(55K-22K) film with 8wt% IL showed some clear phase separation but no orientation. The AFM phase image and GISAXS scattering pattern supported that claim. The cylinders were swollen and the in-plane scattering profile showed too small of a q_y value.

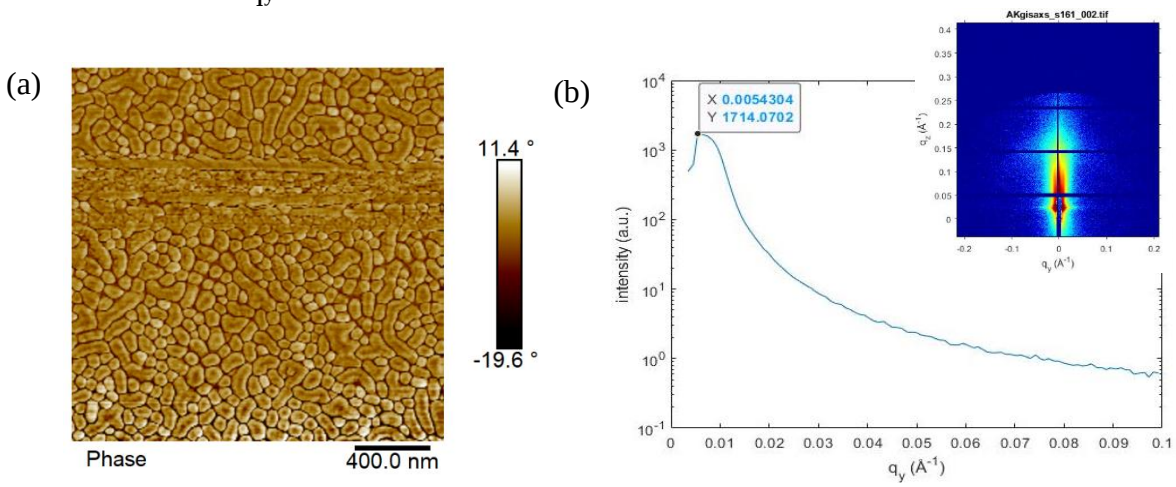

Figure 52: (a) AFM scan image and (b) In-plane scattering profiles of horizontal cut of inset 2D GISAXS pattern of 12wt% IL in 2% PS-*b*-PMMA(55K-22K) DIA film at 40 nm thickness.

DIA 40 nm 2% PS-*b*-PMMA(55K-22K) film with 12wt% IL showed no orientation. The cylinders were swollen and the film had large number of defects. The AFM phase image and GISAXS scattering pattern supported that claim. The in-plane scattering profile showed too small of a q_y value.

Film Thickness: 200 nm

IL (wt%): 0%, 4%, 8%, 12%

DIA solvent mixture – Toluene: Heptane= 1:3 for 30 minutes

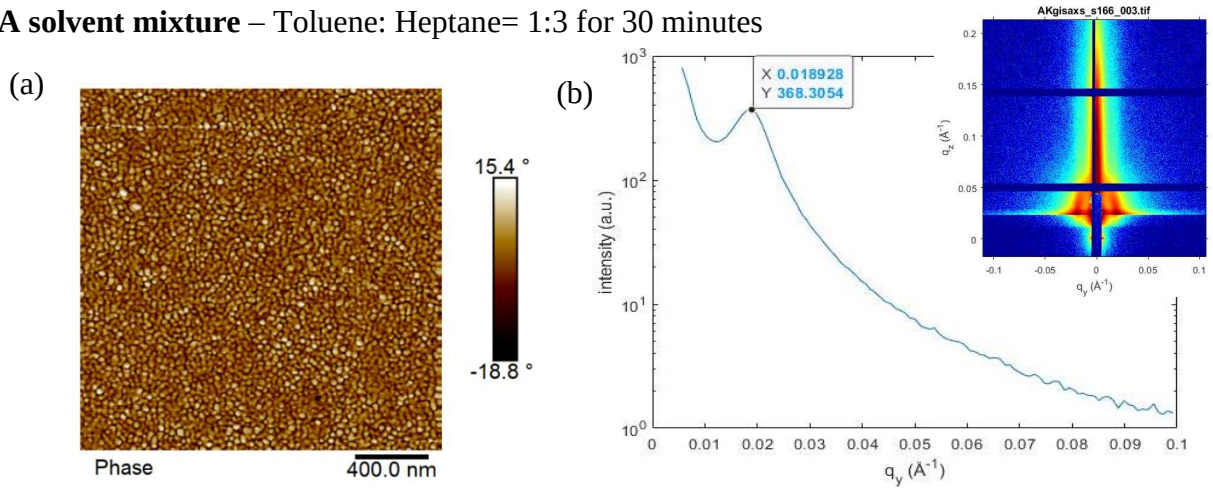

Figure 53: (a) AFM scan image and (b) In-plane scattering profiles of horizontal cut of inset 2D GISAXS pattern of 0wt% IL in 2% PS-*b*-PMMA(55K-22K) DIA film at 200 nm thickness.

DIA 200 nm 2% PS-*b*-PMMA(55K-22K) film without IL showed no significant orientation. The cylinders were swollen and the film had no clear phase separation. The AFM phase image and GISAXS scattering pattern supported that claim. From the in-plane scattering profile the domain spacing was calculated to be 33.2 nm from the q^* of the first order peak.

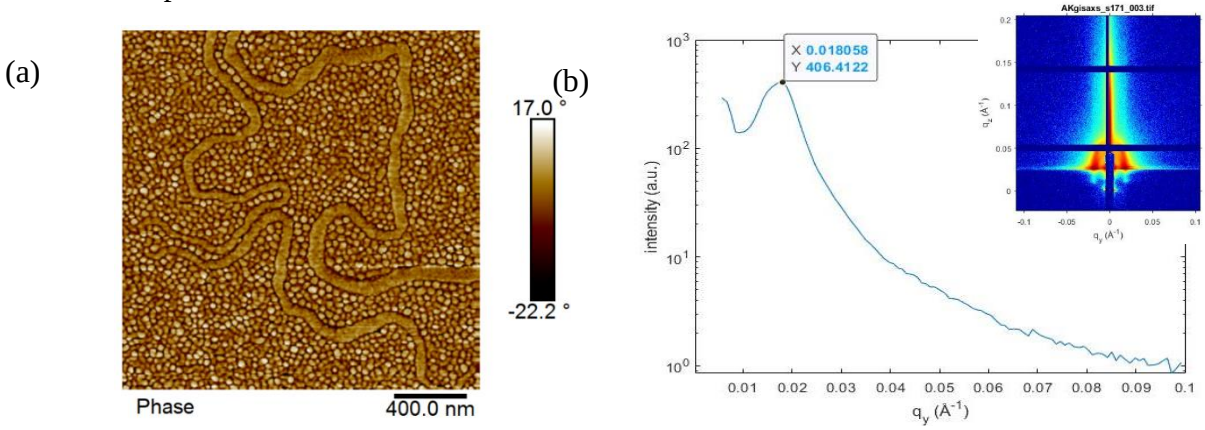

Figure 54: (a) AFM scan image and (b) In-plane scattering profiles of horizontal cut of inset 2D GISAXS pattern of 4wt% IL in 2% PS-*b*-PMMA(55K-22K) DIA film at 200 nm thickness.

DIA 200 nm 2% PS-*b*-PMMA(55K-22K) film with 4wt% IL showed significant vertical orientation with some swollen parallel cylinders on the surface. The AFM phase image and GISAXS scattering pattern supported that claim. From the in-plane scattering profile the domain spacing was calculated to be 35 nm from the q^* of the first order peak.

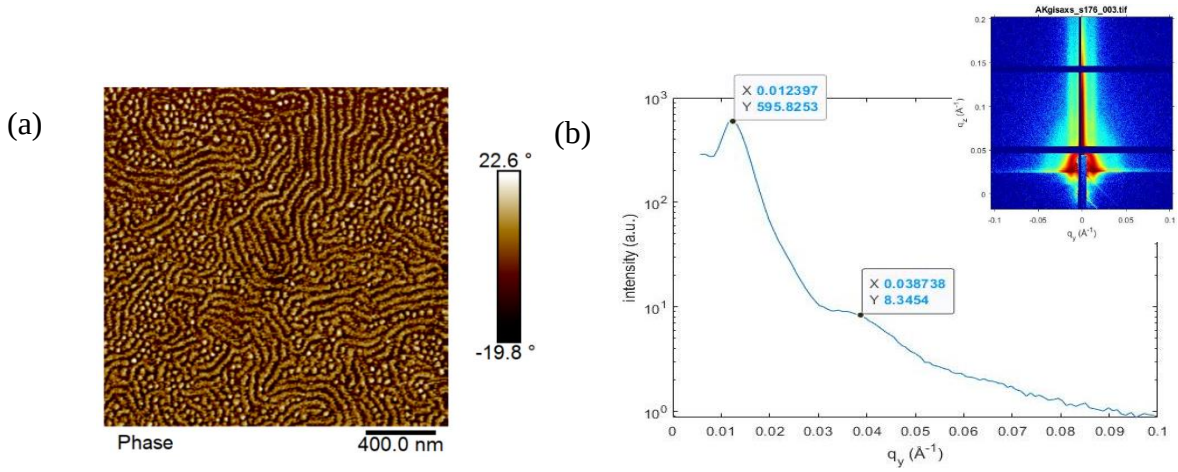

Figure 55: (a) AFM scan image and (b) In-plane scattering profiles of horizontal cut of inset 2D GISAXS pattern of 8wt% IL in 2% PS-*b*-PMMA(55K-22K) DIA film at 200 nm thickness.

DIA 200 nm 2% PS-*b*-PMMA(55K-22K) film with 8wt% IL showed significant in-plane long-range ordering of parallel PMMA cylinders. The cylinders were swollen. The AFM phase image and GISAXS scattering pattern supported that claim. From the in-plane scattering profile the domain spacing was calculated to be 50.7 nm and 16.2 nm from the q^* of the first order peak and the higher order peak, respectively. The ratio is close to ratio of 3:1 but the 2D GISAXS pattern indicated to no existence of perpendicular ordering.

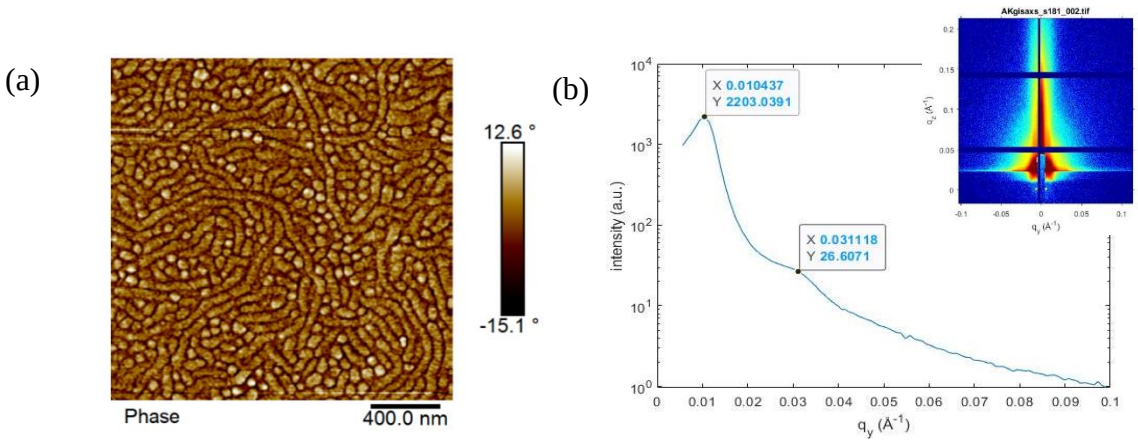

Figure 56: (a) AFM scan image and (b) In-plane scattering profiles of horizontal cut of inset 2D GISAXS pattern of 12wt% IL in 2% PS-*b*-PMMA(55K-22K) DIA film at 200 nm thickness.

DIA 200 nm 2% PS-*b*-PMMA(55K-22K) film with 12wt% IL showed significant mixed orientation. The cylinders were swollen and the meandering of the chains were visible. The AFM phase image and GISAXS scattering pattern supported that claim. From the in-plane scattering profile the domain spacing was calculated to be 62.8 nm and 20.3 nm from the q^* of the first order peak and the higher order peak, respectively. The ratio is close to ratio of 3:1 but the 2D GISAXS pattern indicated to no existence of perpendicular ordering.

Film Thickness: 400 nm

IL (wt%): 0%, 4%, 8%, 12%

DIA solvent mixture – Toluene: Heptane= 1:3 for 30 minutes

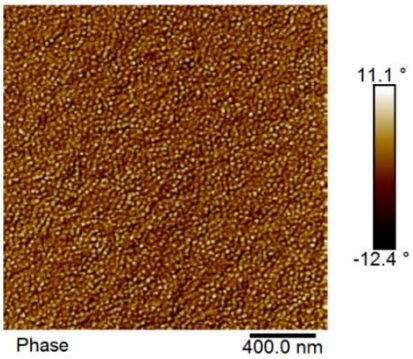

Figure 57: AFM scan image of 0wt% IL in 2% PS-*b*-PMMA(55K-22K) DIA film at 400 nm thickness.

The AFM phase image of DIA 400 nm 2% PS-*b*-PMMA(55K-22K) film without any IL showed phase separation to some extent but the ordering was not significant.

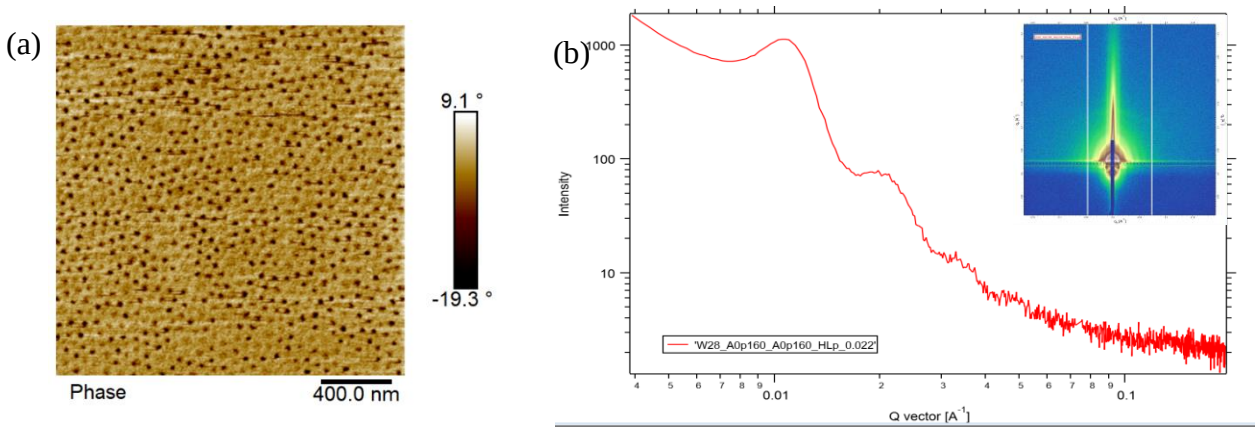

Figure 58: (a) AFM scan image and (b) In-plane scattering profiles of horizontal cut of inset 2D GISAXS pattern of 4wt% IL in 2% PS-*b*-PMMA(55K-22K) DIA film at 400 nm thickness.

The AFM phase image of DIA 400 nm 2% PS-*b*-PMMA(55K-22K) film with 4wt% IL surely showed phase separation but the orientation was mixed. The PMMA cylinders were swollen and opened up pores. From the in-plane scattering profile the domain spacing was calculated to be 62.8 nm and 20.3 nm from the q^* of the first order peak and the higher order peak, respectively. The ratio is close to ratio of 3:1 but the 2D GISAXS pattern indicated to no existence of perpendicular ordering.

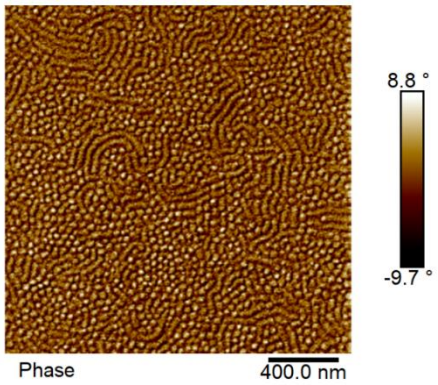

Figure 59: AFM scan image of 8wt% IL in 2% PS-*b*-PMMA(55K-22K) DIA film at 400 nm thickness.

The AFM phase image of DIA 400 nm 2% PS-*b*-PMMA(55K-22K) film with 8wt% IL clearly showed phase separation but the in-plane long-range ordering of parallel cylinders. The PMMA cylinders were swollen.

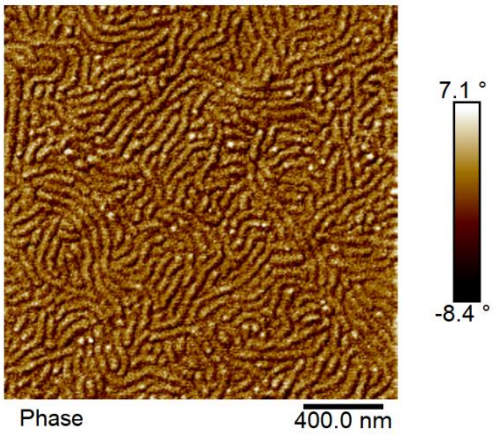

Figure 60: AFM scan image of 12wt% IL in 2% PS-*b*-PMMA(55K-22K) DIA film at 400 nm thickness.

The AFM phase image of DIA 400 nm 2% PS-*b*-PMMA(55K-22K) film with 12wt% IL clearly showed phase separation but the PMMA cylinders were swollen and the parallel orientation of the cylinders were prominent on the surface.

CHAPTER V

CONCLUSIONS

Directed self-assembly of block copolymer (BCP) thin films are the stepping stone for advancement in nanotechnology. BCP thin films as the template for numerous nano-scale electronics has been facing challenges for the scale-up process compared to the available techniques. The potential of BCP films lie on controlling the orientation of the self-assembled blocks to perpendicular ordering relative to the substrate.

This work emphasizes on direct immersion annealing (DIA) as a feasible way to enhance ordering rate to stable morphology of the polymer film for its future application. On an attempt to study the morphology of a well-known BCP of cylindrical orientation i.e. PS-*b*-PMMA (55K-22K), a commercially available and most hydrophobic[22] ionic liquid (IL) was added in varying concentration of 0wt% to 15wt% with respect to the mass of BCP taken. Flow coated BCP film of 100 nm thickness with 4wt% IL, 5wt% IL and 12wt% IL showed perpendicular and parallel cylindrical orientation but not all through the thickness examined by UV-ozone etched ablation test. The phase separation was studied using atomic force microscopy (AFM) and the internal film orientation was characterized by grazing incidence small angle X-ray scattering (GISAXS) techniques above the critical angle of the film (0.12°). The surface energy showed typical low energy owing to hydrophobicity of BCP and films with or without IL showed no significant difference in surface energy. The results of 100 nm thickness BCP films led to systematic study of three different thickness of 40 nm, 200 nm and 400 nm with addition of 0wt% IL, 4wt% IL, 8wt% IL and 12wt% IL, respectively. 40 nm thick film didn't show definite

cylindrical ordering. For 200 nm and 400 nm BCP films, one particular IL percentage showed promising ordering i.e., 4wt% IL, revealed by AFM and GISAXS. Ablation test for 400 nm BCP film with 4wt% IL didn't show perpendicular cylindrical orientation throughout the thickness. 100 nm thin films with 0wt% IL, 2wt% IL,4wt% IL, 5wt% IL, 8wt% IL and 12wt% IL additive were studied respectively for direct immersion annealing (DIA) method by immersing the films in a solvent mixture of toluene and heptane of 1:3 ratios for 30 minutes. Similar to as cast films of 4wt% IL, 5wt% IL and 12wt% IL additive, the annealed films showed better orientation in this particular solvent mixture. Then 12wt% IL added 100 nm thick film was subjected to different ratios of 1:2, 1:3, 1:6 and 1:9 of toluene and heptane mixture for prolonged time of 2 hours for annealing. The ratio of 1:3 showed better result but not as good as 30 minutes' immersion time. That's why annealing time of 30 minutes and immersion mixture of toluene and heptane of 1:3 ratios were chosen for films with IL additive of 0wt%, 4wt%, 8wt% and 12wt% for other three different thickness of 40 nm, 200 nm and 400 nm, respectively. For 40 nm films the ordering was not prominent. As for 200 nm and 400 nm films, the 4wt% IL film showed the best vertical cylindrical ordering. Films with 8wt% IL and 12wt% IL showed long-range in-plane ordering of parallel cylinders.

Future Work

A more detailed analysis on the concentration or loading of IL in the PS-*b*-PMMA (55K-22K) matrix will enrich the study and it will give more understanding of the mobility of IL and its role on changing the interfacial energy.[7, 23] Time-of-Flight Secondary Ion Mass Spectrometry (ToF-SIMS) could be used to determine the loading of IL in PMMA cylinders where a pulsed ion beam removes the surface of a film and

analyzes the ejected secondary ions. Glass transition temperature, T_g of the polymer-IL matrix blend could also be determined by differential scanning calorimetry.[24] The cylindrically ordered film could be the substrate for nano-patterning.[25] This polymer-IL blend could be the next generation building block for nanolithography.[26] Nanoporous thin film of PS-b-PMMA as an upper layer membrane prepared by selectively removing the PMMA block by UV irradiation followed by rinsing with acetic acid and supported by a strong membrane could be a potential filtration membrane for protein separation or water purification.[27, 28] A comparative study of other IL in this particular block copolymer system is also of interest.[29] Neutron reflectivity data could help on detailed study on interfacial width and domain size induced by selective DIA solvent mixture. This system can be studied for potential polymer electrolyte on a metal coated substrate.[30]

REFERENCES

(1) Albert, J. N.L.; Epps, T.H. Self-assembly of block copolymer of thin films. *Materials Today* **June 2010**, *13.*

(2) Modi, A.; Bhaway, S. M.; Vogt, B. D.; Douglas, J. F.; Al-Enizi, A.; Elzatahry, A.; Sharma, A.; Karim, A. Direct Immersion Annealing of Thin Block Copolymer Films. *ACS Appl. Mater. Interfaces* **2015**, *7*, 21639−21645.

(3) Longanecker, M.; Modi, A.; Dobrynin, A.; Kim, S.; Yuan, G.; Jones, R.; Sajita, S.; Bang, J.; Karim, A. Reduced Domain Size and Interfacial Width in Fast Ordering Nanofilled Block Copolymer Films by Direct Immersion Annealing. *Macromolecules* **2016**, *49*, 8563−8571.

(4) Tamate, R.; Hashimoto, K.; Ueki, T.; Watanabe, M. Block copolymer self-assembly in ionic liquids. *Phys. Chem. Chem. Phys.* **2018**, *20*, 25123-25139.

(5) Sinturel, C.; Bates, F. S.; Hillmyer, M. A. High χ − Low N Block Polymers: How Far Can We Go? *ACS Macro. Lett.* **2015**, *4*, 1044-1050.

(6) Segalman, R. A. Patterning with block copolymer thin films. *Materials Science and Engineering R* **2005,** *48*, 191–226.

(7) Chen, X.; Zhou, C.; Chen, S.; Craig, G.; Rincon-Delgadillo, P.; Dazai, T.; Miyagi, K.; Maehashi, T.; Yamazaki, A.; Gronheid, R.; Stoykovich, M. P.; Nealey, P. F. Ionic Liquids as Additives to Polystyrene-Block-Poly (Methyl Methacrylate) Enabling Directed Self-Assembly of Patterns with Sub-10 nm Features. *ACS Appl. Mater. Interfaces* **2018**, *10*, 16747−16759.

(8) Son, C. Y.; McDaniel, J. G., Cui, Q.; Yethiraj, A. Conformational and Dynamic Properties of Poly(ethylene oxide) in $BMIM^{+}BF_4^{-}$: A Microsecond Computer

Simulation Study Using ab Initio Force Fields. *Macromolecules* **2018**, *51*, 5336−5345.

(9) Liu, Z.; Wang, W.; Stadler, F. J.; Yan, Z. Rheology of Concentrated Polymer/Ionic Liquid Solutions:An Anomalous Plasticizing Effect and a Universality in Nonlinear Shear Rheology. *Polymers* **2019**, *11*, 877.

(10) Park, W. I.; Kim, J. M.; Jeong, J.; Jung, Y.S. Deep-Nanoscale Pattern Engineering by Immersion-Induced Self-Assembly. *ACS Nano* **2014,** *8*, 10009-10018.

(11) Morris, W.G. Atomic Force Microscopy. In *Encyclopedia of Materials: Science and Technology*; 2nd ed.; Elsevier Pergamon: Netherlands, **2001**; p 1-6.

(12) Nayfeh, M. Characterization and Simulation Technologies of Nanomaterial. In *Fundamentals and Applications of Nano Silicon in Plasmonics and Fullerines*; 1st ed.; Elsevier: Netherlands, **2008**; p 153-156.

(13) Swift, C. The Opensource Handbook of Nanoscience and Nanotechnology [Online]; Wikibooks, **2019**. https://en.wikibooks.org/wiki/Nanotechnology/AFM (accessed March 31, 2020).

(14) Bergström, J. Experimental Characterization Techniques. In *Mechanics of Solid Polymers*; 1st ed.; Elsevier William Andrew: Netherlands, **2015**; p 19-114.

(15) Yang, S.; Park, J.; Yoon, J.; Ree, M.; Jang, S.; Kim, J. Virus Filtration Membranes Prepared from Nanoporous Block Copolymers with Good Dimensional Stability under High Pressures and Excellent Solvent Resistance. *Adv. Funct. Mater.* **2008**, *18*, 1371–1377.

(16) Renauda, G.; Lazzari, R.; Leroy, F.; Probing Surface and Interface Morphology with Grazing Incidence Small Angle X-Ray Scattering. *Surface Science Reports*,

2009, *64***,** 255–380.

(17) Anastasiadis, S.H.; Russell, T.P.; Satija, S.K.; Majkrzak, C. F.; Neutron reflectivity studies of the surface-induced ordering of diblock copolymer films. *Phys. Rev. Lett.* **1989**, *62*, 1852-1855.

(18) Als-Nielsen, J.; McMorrow, D. Elements of Modern X-ray Physics. John Wiley & Sons: New York, **2001.**

(19) Fowkes, F. M. Attractive Forces at Interfaces. *Ind. Eng. Chem*. **1964,** *56*, 40–52

(20) Modi, A.; Karim, A.; Tsige, M. Solvent and Substrate Induced Synergistic Ordering in Block Copolymer Thin Films. *Macromolecules* **2018**, *51*, 7186−7196.

(21) Hansen Solubility Parameters. https://www.hansen-solubility.com/HSP-science/basics.php (accessed April 20, 2020).

(22) Ye, Y.S.; Rick, J.; Hwang, B.J. Ionic Liquid Polymer Electrolytes. *J. Mater. Chem. A* **2013**, *1 (8)*, 2719–2743.

(23) Chen, S.; Wu,G,; Wang, X.; Chen, X.; Nealey, P.F. Sub-10 nm Feature Sizes of Disordered Polystyrene-blockpoly(methyl methacrylate) Copolymer Films Achieved by Ionic Liquid Additives with Selectively Distributed Charge Interactions. *ACS Appl. Polym. Mater*. **2020**, *2*, 427−436.

(24) Bennett, T. M.; Pei, K.; Cheng, H.; Thurecht, K.; Jack, K. S.; Blakey, I. Can ionic liquid additives be used to extend the scope of poly(styrene)-block-poly(methyl methacrylate) for directed self-assembly? *J. Micro/Nanolith. MEMS MOEMS* **2014**, *13(3)*, 031304.

(25) Cheng, J.Y.; Mayes, A. M.; Ross. C. A. Nanostructure engineering by templated self-assembly of block copolymers. *Nature Materials*, November **2004**, *Vol 3*, 823-

828.

(26) Jeong, S. J.; Kim, J. Y.; Kim, B. H.; Moon, H.S.; Kim, S.O. Directed self-assembly of block copolymers for next generation nanolithography. *Materials Today* December **2013**, Volume 16, Number 12, 469-476.

(27) Sofia, R.; Buhr, K.; Filiz, V.; Clodt, J. I.; Lademann, B.; Hahn, J.; Jung, A.; Abertz, V. Self-organized isoporous membranes with tailored pore sizes. *J. Memb. Sci.* **2014,** *451*, 266–275.

(28) Phillip, W. A.; Neill, B. O.; Rodwogin, M.; Hillmyer, M. A.; Cussler, E. L. Self-Assembled Block Copolymer Thin Films as Water Filtration Membranes. *ACS Appl. Mater. Interfaces* **2010**, *2* (3), 847–853.

(29) Bennett, T. M.; Chambers, L.C.; Cheng, H.; Thurecht, K.; Jack, K. S.; Blakey, I. Dependence of Block Copolymer Domain Spacing and Morphology on the Cation Structure of Ionic Liquid Additives. *Macromolecules* **2018**, *51*, 8979−8986.

(30) Kambe, Y.; Arges, C. G.; Czaplewski, D. A.; Dolejsi, M.; Krishnan, S.; Stoykovich, M. P.; de Pablo, J. J.; Nealey, P. F. Role of Defects in Ion Transport in Block Copolymer Electrolytes. *Nano Lett*. **2019**, *19*, 7, 4684-4691.